

Parameterizing and constraining scalar corrections to general relativity

Leo C. Stein*

Center for Radiophysics and Space Research, Cornell University, Ithaca, NY 14853 USA

Kent Yagi†

Department of Physics, Montana State University, Bozeman, MT 59717 USA

(Dated: August 12, 2022)

We parameterize a large class of corrections to general relativity which include a long-ranged gravitational scalar field as a dynamical degree of freedom in two ways: parameterizing the structure of the correction to the action, and parameterizing the scalar hair (multipole structure) that compact objects and black holes attain. The presence of this scalar hair violates the no-hair theorems present in general relativity, which leads to several important effects. The effects we consider are i) the interaction between an isolated body and an external scalar field, ii) the scalar multipole-multipole interaction between two bodies in a compact binary, iii) the additional pericenter precession of a binary, iv) the scalar radiation from a binary, and v) the modification to the gravitational wave phase from a binary. We apply this framework to example theories including Einstein-dilaton-Gauss-Bonnet gravity and dynamical Chern-Simons gravity, and estimate the size of the effects. Finally we estimate the bounds that can be placed on parameters of the theories from the precession of pulsar binaries and from gravitational waves.

PACS numbers: 04.50.Kd, 04.25.Nx

I. INTRODUCTION

General relativity is known to be consistent with all experimental and observational tests to date [1, 2]. However, all of these tests are in the weak-field, low-curvature, and low-velocity regime of the theory. According to the modern paradigm of effective field theories, we expect GR to require corrections at a yet-unexplored curvature scale, associated with some new length scale. In the regime where these corrections are small, they can be explored by perturbing away from known GR solutions.

One of the most commonly explored extensions of general relativity is that of a theory with both a metric and a scalar, motivated by fundamental or effective field theories. In such theories, a “gravitational” scalar is 1) long ranged and 2) couples weakly. Such a theory must reduce to GR in the weak-field, slow-motion limit, so that the scalar is negligible in the Solar System, and thus evades weak-field tests. Some examples of such theories are Brans-Dicke [1, 2], Einstein-dilaton-Gauss-Bonnet (EDGB) gravity [3, 4], and dynamical Chern-Simons (dCS) gravity [5, 6].

A common theme in these theories is that stationary compact objects, such as neutron stars (NSs) and/or black holes (BHs), act as effective sources of the long-ranged scalar field, acquiring scalar charge (called “hair” for BHs). The presence of this scalar charge violates the no-hair theorems of GR for black holes. For neutron stars the scalar field strength can depend on the internal structure

of the star, which violates the principle of effacement.¹ The magnitude of this scalar charge depends on the size and mass of the body in relation to the new length scale.

The presence of this scalar field modifies dynamics of a compact binary system in both the conservative and dissipative sectors. Consequently, a binary experiences additional pericenter precession, and the gravitational wave signature is modified. Both of these effects are observable and therefore can be used to constrain the coupling strength (which can be quantified through a length ℓ) of the scalar interaction in this type of theory.

In this Paper we parameterize the types of scalar interactions and the multipole structure acquired by BHs and NSs. Using this parameterization we calculate observable effects in a compact binary system (the additional pericenter precession and modification to gravitational wave phase). Using these observables and the estimated scaling laws for scalar multipole moments in this class of theories, we are able to estimate the bounds which can be placed on the coupling strength of the non-minimal scalar interaction of these theories.

We find a specific power-law scaling for the estimated bound on ℓ in terms of the binary orbital velocity, with the power determined by the parameterization of the theory. The pericenter precession bound improves (goes to shorter lengths) with higher-velocity binaries. Gravitational waves are estimated to provide an even stronger constraint than pulsar binaries. Gravitational waves from

¹ The effacement principle in GR says that at low order, a gravitational body may be described as a point particle with the same mass [7]. In the post-Newtonian expansion, finite-size effects enter at 5pN order [8], while in the extreme mass-ratio limit they enter at fourth order in the mass ratio [9].

* Einstein fellow; leostein@astro.cornell.edu

† kyagi@physics.montana.edu

comparable mass-ratio binaries with stellar masses are estimated to provide bounds on the order of the gravitational lengths present in the system: a combination of the gravitational radii, extents of the bodies, and their separations. For NS-NS binaries this gives a typical length at the kilometer scale.

The plan for this paper is as follows. In Sec. II, we lay out the two parameterizations we use in this paper. In Sec. III, we lay out the multipole structure of the scalar field of an isolated compact object, a compact binary system, and the scalar radiation field thereof. In Sec. IV we estimate the scalings of scalar multipole moments of compact objects, which leads to scaling estimates of scalar multipoles of a compact binary system. In Sec. V we derive the scalar field-pole interaction and force on an isolated body, and the scalar pole-pole interaction and force in a compact binary system. In Sec. VI we compute the additional pericenter precession in a binary due to the pole-pole interaction. In Sec. VII we compute the radiation reaction due to the flux produced by the binary. In Sec. VIII we compute the modification to the gravitational wave signature and the parameterized post-Einsteinian parameters. In Sec. IX we estimate the bounds which could be placed from pericenter precession and gravitational wave measurements. We conclude in Sec. X.

II. PARAMETERIZATION OF THEORIES

Throughout, we will work in units $c = 1 = \hbar$ where $[L] = [T] = [M]^{-1}$, and recall that $(8\pi G)^{-1} = m_{\text{pl}}^2$ so $[G] = [L]^2$. We take the scalar θ to have length dimensions $[\theta] = [L]^{-1}$, so the dimensions of its source are $[\tau] = [L]^{-3}$. From the structure of the multipolar expansion, an s -pole tensor μ^S has length dimensions $[\mu^S] = [L]^s$.

We take the full action to be given by the Einstein-Hilbert action for gravity, a canonical kinetic term for the scalar field, a non-minimal interaction term between the scalar field and gravity, and a matter term:

$$S = S_{\text{EH}} + S_{\text{kin}} + S_{\text{int}} + S_{\text{mat}} \quad (1)$$

$$S_{\text{EH}} = \int \frac{1}{2} m_{\text{pl}}^2 R \sqrt{-g} d^4x \quad (2)$$

$$S_{\text{kin}} = \int -\frac{1}{2} (\partial_a \theta) (\partial^a \theta) \sqrt{-g} d^4x \quad (3)$$

$$S_{\text{int}} = \int \mathcal{L}_{\text{int}}[\theta, g, \epsilon, \nabla, R] \sqrt{-g} d^4x. \quad (4)$$

A more general action would include a potential for the scalar, but in order to treat the scalar as “gravitational,” we take the potential to be flat so that the scalar is long-ranged. We work in the Jordan frame where matter fields couple minimally to the metric, so the scalar field does not appear in the matter action. This is appropriate since higher-curvature and higher-derivative actions may not be conformally transformed to the Einstein frame [10].

We expand the interaction term \mathcal{L}_{int} in powers of θ . For the purposes of this paper, we are interested in the linear part: the part with no powers of θ is not an interaction, so the linear part leads in the expansion; and it would require fine-tuning for there to be no linear piece. In this work we study only the linear-in- θ interaction. This may always be written as

$$\mathcal{L}_{\text{int}} \sim \theta T[g, \epsilon^{0,1}, \nabla, R] \quad (5)$$

via integration by parts to remove all derivatives from θ . Here T is a tensor constructed from the metric, zero or one epsilon tensors,² the Levi-Civita connection of the metric and its curvature. At the linear order, the contribution to the scalar field coming from different types of operators within T will simply superimpose. Therefore we will study each type of term separately by considering only

$$\mathcal{L}_{\text{int}} \sim \theta T[g, \epsilon^{0,1}, \nabla^d, R^r] \quad (6)$$

which is built from d covariant derivatives and r curvature tensors. By counting indices, d must be even in four dimensions.

It's clear that we must introduce a new length scale, ℓ , related to a cutoff of the effective field theory. This length scale quantifies the strength of this interaction Lagrangian and the curvature radius where the interaction becomes important. There are several ways to parameterize this length (including in terms of a cutoff—see App. A). For future convenience we choose

$$\mathcal{L}_{\text{int}} \sim (m_{\text{pl}} \ell)^{\wp} \theta T[g, \epsilon^{0,1}, \nabla^d, R^r] \quad (7)$$

where for dimensional correctness we have

$$\wp = d + 2r - 3. \quad (8)$$

Thus the parameterization of the scalar interaction is given by the integers $(|\epsilon|, d, r)$ (where $|\epsilon| = 0, 1$ counts the appearance of ϵ tensors).

This interaction term is responsible for sourcing the scalar field, in its equation of motion

$$\square \theta = -4\pi \tau \quad (9)$$

where clearly $\tau \sim (m_{\text{pl}} \ell)^{\wp} T[g, \epsilon^{0,1}, \nabla^d, R^r]$. This equation must be solved in the curved strong-field region. However in the far field, through asymptotic matching, the source term can be replaced with an effective source term (for example, see [11, 12] and for a more general discussion see [13]). The far field solution will be dominated by some lowest non-vanishing scalar multipole moment, which has a corresponding effective source term which we discuss in Sec. III.

The non-vanishing scalar moment of lowest multipole order dominates much of the phenomenology associated

² Exactly zero or one epsilon tensors may appear, owing to the identity $\epsilon^{i_1 \dots i_n} \epsilon_{j_1 \dots j_n} = (\text{sgn } g) n! \delta_{j_1}^{i_1} \dots \delta_{j_n}^{i_n}$.

Theory	$ \epsilon $	d	r	\wp^a	ℓ_{BH}	ℓ_{NS}	$\ell_{\text{rad}}^{\text{HH}}$	$\ell_{\text{rad}}^{\text{HS}}$	$\ell_{\text{rad}}^{\text{SS}}$
“Scalar-Tensor”	0	0	1	-1	— ^b	0	— ^b	1	1
EDGB	0	0	2	1	0	2 ^c	1	1	3 ^c
dCS	1	0	2	1	1	1	2	2	2

^a Not independent, $\wp = 2r + d - 3$.

^b Black holes have no hair in classical scalar-tensor theories.

^c This is expected but has not yet been calculated.

TABLE I. Parameters of three example theories with a long-ranged, weakly-coupling “gravitational” scalar. The interaction Lagrangians are seen in Eq. (10). The parameter of the Lagrangian are $(|\epsilon|, d, r)$, and the multipole parameters are $(\ell_{\text{BH}}, \ell_{\text{NS}}, \ell_{\text{rad}})$. In this table we have $\ell_{\text{rad}} = 1 + \min(\ell_1, \ell_2)$, as suggested in Sec. III B.

with the scalar field. The scalar structure must be determined on a per-theory basis through asymptotic matching to a genuine strong-field solution. For the purposes of this paper, we simply parameterize it by some integers. We will take a NS to have scalar multipole tensors μ_{NS}^S with S a multi-index of valence $s = |S|$, i.e. $S = k_1 \cdots k_s$. The first few of these may identically vanish; the lowest non-vanishing one is numbered with $s = \ell_{\text{NS}}$. Similarly, a black hole has scalar multipole tensors μ_{BH}^H , and the lowest non-vanishing tensor is numbered with $h = \ell_{\text{BH}}$.

The scalar multipole moments of a compact binary system, μ_{bin}^B , are determined directly from the moments of the constituent bodies μ_A^I (with $A = 1, 2$) and their orbits (see Sec. III B). In a compact binary (consisting of BH-BH, BH-NS or NS-NS) the lowest non-vanishing scalar moment of the binary is simply the lower of the two constituents, $\ell_{\text{bin}} = \min(\ell_1, \ell_2)$.

The motion of the binary will lead to scalar radiation, now with radiative multipoles which are determined directly from (time derivatives of) the binary moments μ_{bin}^W (see Sec. III B). However, the lowest non-vanishing binary source multipole might not be responsible for the dominant radiation, for example if there is a conservation law that protects certain multipoles. Therefore we also parameterize the *dominant* radiation multipole as $\ell_{\text{rad}} \geq \ell_{\text{bin}}$. In fact the dominant radiative multipole can differ for BH-BH, BH-NS, and NS-NS binaries. We will suggest in Sec. III B that the dominant radiative multipole is $\ell_{\text{rad}} = 1 + \ell_{\text{bin}} = 1 + \min(\ell_1, \ell_2)$. The parameterization of the multipole structure of the theory is then given by the integers $(\ell_{\text{NS}}, \ell_{\text{BH}}, \ell_{\text{rad}})$ with $\ell_{\text{rad}}^{\text{HH}}, \ell_{\text{rad}}^{\text{HS}}, \ell_{\text{rad}}^{\text{SS}}$ for respectively BH-BH, BH-NS, and NS-NS binaries.

The full parameters of a theory, then, are given by $(|\epsilon|, d, r, \ell_{\text{BH}}, \ell_{\text{NS}}, \ell_{\text{rad}})$. We give these parameters for a sampling of theories in Table I. The theories which we highlight are classical “scalar-tensor” theories, dynamical Chern-Simons (dCS), and Einstein-dilaton-Gauss-Bonnet (EDGB). The leading interaction terms for those theories

are

$$\mathcal{L}_{\text{int}}^{\text{S-T}} \sim m_{\text{pl}} \theta R \quad (10a)$$

$$\mathcal{L}_{\text{int}}^{\text{dCS}} \sim m_{\text{pl}} \ell^2 \theta {}^*RR \quad (10b)$$

$$\mathcal{L}_{\text{int}}^{\text{EDGB}} \sim m_{\text{pl}} \ell^2 \theta {}^*R{}^*R \quad (10c)$$

where the (left-)dual Riemann tensor is

$${}^*R^{abcd} = \frac{1}{2} \epsilon^{abef} R_{ef}{}^{cd} \quad (11)$$

(and similarly for the Weyl tensor C), the Pontryagin density is

$${}^*RR = {}^*R^{abcd} R_{abcd} = {}^*C^{abcd} C_{abcd} \quad (12)$$

and the 4-dimensional Euler (or Gauss-Bonnet) density is

$${}^*R{}^*R = {}^*R^{abcd} {}^*R_{abcd}. \quad (13)$$

Each of these three theories has $\ell_{\text{rad}} = 1 + \min(\ell_1, \ell_2)$.

III. MULTIPOLE MOMENTS

We devote this section to the formalism of the latter half of the parameterization, that of the scalar multipole structure of isolated bodies, compact object binaries, and scalar radiation fields. The formalism uses the machinery of symmetric trace-free (STF) tensors; for references, see e.g. [14–16].

A. Isolated stationary compact object

Exterior to an isolated stationary compact object, the scalar field will be dominated by some lowest non-vanishing multipole moment giving rise to a solution of the form

$$\theta_*^{\text{WF}} = \mu_*^S \partial_S \frac{1}{r_*} \quad (14)$$

where a sub- or superscript asterisk refers to a property of a star (or BH), here the scalar field of a body θ_* , multipole moment of a body μ_* , and field point distance to a body r_* . This solution is to be found from a numerical or analytic solution in the strong-field and extracting the slowest-decaying behaviour in the weak-field (WF). We would like to approximate this with an effective point-particle source on flat space-time, i.e. to perform an asymptotic matching. On flat space-time, for the scalar equation of motion given in Eq. (9), the solution would be found from the Green’s function for \square , given by

$$\theta(t, \mathbf{x}) = \int_{\mathcal{N}} \frac{\tau_{\text{eff}}(t - |\mathbf{x} - \mathbf{x}'|, \mathbf{x}')}{|\mathbf{x} - \mathbf{x}'|} d^3x' \quad (15)$$

where \mathcal{N} is the intersection of the past light-cone of (t, \mathbf{x}) and the source region (see [16] for details).

The effective point-particle source which reproduces Eq. (14) is given simply by

$$\tau_{\text{eff}} = (-)^s \mu_*^S \partial_S \delta^{(3)}(\mathbf{x} - \mathbf{x}_*). \quad (16)$$

This can be verified directly by inserting Eq. (16) into Eq. (15) and integrating by parts s times.

B. Binary and radiation multipoles

The far-zone solution for θ is given by an expansion of Eq. (15) for large r , which is given by [16]

$$\theta = \sum_{q=0}^{\infty} \frac{(-)^q}{q!} \left(\frac{1}{r} \mu_{\text{bin}}^Q \right)_{,Q} \quad (17)$$

where

$$\mu_{\text{bin}}^Q(u) = \int_{\mathcal{M}} \tau_{\text{eff}}(u, \mathbf{x}) x^Q d^3x \quad (18)$$

are the source multipoles, $u = t - r$ the retarded time, \mathcal{M} the constant- t hypersurface intersecting the world tube, and where $x^Q = x^{k_1} \dots x^{k_q}$. Here $\tau_{\text{eff}} = \tau_{\text{eff},1} + \tau_{\text{eff},2}$ is the superposition of the effective source terms for bodies 1 and 2 on a Keplerian orbit. Thus multipole moments of the binary are determined from the multipole moments of the constituent bodies, μ_A^S with $A = 1, 2$, at positions \mathbf{x}_A . Superposing the two effective source terms [Eq. (16)] and evaluating the source multipole integral [Eq. (18)] gives

$$\begin{aligned} \mu_{\text{bin}}^Q &= \mu_1^S \int \delta^{(3)}(\mathbf{x} - \mathbf{x}_1) x^Q_{,S} d^3x + (1 \leftrightarrow 2) \quad (19) \\ \mu_{\text{bin}}^Q &= \begin{cases} \frac{q!}{s!} \mu_1^{(k_1 \dots k_s k_{s+1} \dots k_q)} + (1 \leftrightarrow 2) & q \geq s \\ 0 & \text{otherwise} \end{cases} \quad (20) \end{aligned}$$

where $+(1 \leftrightarrow 2)$ means to add the same expression with labels 1 and 2 exchanged. This has been written as if $\ell_1 = \ell_2$, which is valid for BH-BH or NS-NS binaries, but the extension to $\ell_1 \neq \ell_2$ should be clear. Evaluating these moments requires the identity

$$x^Q_{,S} = \begin{cases} \frac{q!}{s!} \delta_S^{(k_1 \dots k_s k_{s+1} \dots k_q)} & q \geq s \\ 0 & \text{otherwise} \end{cases} \quad (21)$$

where $\delta_A^B = \delta_{a_1}^{b_1} \dots \delta_{a_q}^{b_q}$ with $|A| = |B| = q$. The salient feature here is that the q^{th} binary source moment contains $\max(0, q - \ell_A)$ powers of x_A^k .

In the far zone, the scalar field solution is radiative. The derivatives in Eq. (17) act on both $1/r$ and each $\mu_{\text{bin}}^Q(u)$ which depends on retarded time. The solution which dominates has all derivatives acting on $\mu_{\text{bin}}^Q(u)$, since any derivatives which act on $1/r$ introduce additional powers of $1/r$. Further, when a spatial derivative acts on a quantity which depends only on retarded time, we have

$$\frac{\partial}{\partial x^i} F(u) = -n^i \frac{\partial}{\partial t} F(u) \quad (22)$$

with n^a the unit normal direction vector from the origin to some field point. Thus the dominant term is

$$\theta_{\text{rad}} = \sum_{q=\ell_{\text{bin}}}^{\infty} \frac{1}{r} \frac{n^Q}{q!} {}^{(q)}\mu_{\text{bin}}^Q(u) \quad (23)$$

where $n^Q = n^{k_1} \dots n^{k_q}$ and where ${}^{(q)}f = (\partial/\partial t)^q f$. However, there may be a conservation law or a suppression for $q = \ell_{\text{bin}}$. Therefore to be slightly more general, we let the radiation have a lowest non-vanishing moment ℓ_{rad} , so the dominant term is

$$\theta_{\text{rad}} = \frac{1}{r} \frac{n^W}{w!} {}^{(w)}\mu_{\text{bin}}^W(u) \quad (24)$$

where $w = |W| = \ell_{\text{rad}}$.

In particular, focus on the lowest non-vanishing source moment μ_{bin}^B with $|B| = \ell_{\text{bin}} = \min(\ell_1, \ell_2)$. In this case, the binary source multipole tensor contains zero powers of the positions of the bodies; it is simply $\mu_{\text{bin}}^B = \mu_1^B + \mu_2^B$ which contains no powers of x_A^i . Clearly, time derivatives of this moment are ${}^{(n)}\mu_{\text{bin}}^B = {}^{(n)}\mu_1^B + {}^{(n)}\mu_2^B$. These time derivatives depend on changes to the internal structure of the bodies, or at best, if a moment depends on the spin of a body, on the precession of that spin. Both of the associated time scales are long compared to the orbital time. In contrast, consider the next highest moment, $1 + \ell_{\text{bin}}$. In the case of $\ell_1 = \ell_2$, we have for the $1 + \ell_1$ moment

$$\mu_{\text{bin}}^{aS} = w x_1^a \mu_1^S + (1 \leftrightarrow 2) \quad (25)$$

with $|S| = \ell_1$, whereas for, say, $\ell_1 < \ell_2$ we have simply

$$\mu_{\text{bin}}^{aS} = w x_1^a \mu_1^S. \quad (26)$$

This already contains one power of position vectors, and so it will vary on the orbital time scale, rather than the precession or radiation-reaction time scale. For this reason, we suggest that $\ell_{\text{rad}} = 1 + \ell_{\text{bin}}$ will be the dominant radiative scalar moment in most cases.

In this case, as we can see from Eq. (24), we need to compute $1 + \ell_1$ time derivatives of μ_{bin}^{aS} from Eq. (25) or Eq. (26) if respectively $\ell_1 = \ell_2$ or $\ell_1 < \ell_2$. Let us rewrite this on a Kepler orbit using $\mathbf{x}_1 = (m_2/m)\mathbf{x}_{12}$, $\mathbf{x}_2 = -(m_1/m)\mathbf{x}_{12}$ where m_A is the mass of particle A , $m = m_1 + m_2$ is the total mass, and $\mathbf{x}_{12} = \mathbf{x}_1 - \mathbf{x}_2$ is the directed relative separation vector. Then we have

$$\mu_{\text{bin}}^{aS} = w x_{12}^a \left[\frac{m_2}{m} \mu_1^S - \frac{m_1}{m} \mu_2^S \right]. \quad (27)$$

For future brevity we now define

$$\mu_{\text{red}}^S \equiv \left[\frac{m_2}{m} \mu_1^S - \frac{m_1}{m} \mu_2^S \right] \quad (28)$$

which is akin to a ‘‘reduced’’ moment.

Now consider some number of time derivatives of this tensor. Any time derivatives acting on μ_A^S are, by assumption, suppressed by the ratio of the orbital time to the

precession time. Therefore we can consider all of the time derivatives acting on x_{12}^a , which is simply

$$\frac{\partial}{\partial t} x_{12}^a = v_{12}^a \quad (29)$$

the directed relative velocity vector, $\mathbf{v}_{12} = \mathbf{v}_1 - \mathbf{v}_2$. This simplifies for a circular orbit, where

$$\left(\frac{\partial}{\partial t}\right)^2 x_{12}^a = -\omega^2 x_{12}^a = -\frac{Gm}{r_{12}^3} x_{12}^a = -\frac{1}{(Gm)^2} x_{12}^a v^6 \quad (30)$$

where $r_{12} = |\mathbf{x}_{12}|$, ω is the orbital angular frequency, and using the leading Kepler relation ($v^2 = Gm/r_{12}$), where now we write simply v for $|\mathbf{v}_{12}|$. Then in the circular, adiabatic limit, where the time derivative of r_{12} is negligible, we have

$$\left(\frac{\partial}{\partial t}\right)^{2j} x_{12}^a = \frac{(-)^j}{(Gm)^{2j}} x_{12}^a v^{6j} \quad (31a)$$

$$\left(\frac{\partial}{\partial t}\right)^{2j+1} x_{12}^a = \frac{(-)^j}{(Gm)^{2j}} v_{12}^a v^{6j} \quad (31b)$$

with j a non-negative integer. This gives

$${}^{(2j)}\mu_{\text{bin}}^{aS} = \frac{(-)^j w}{(Gm)^{2j-1}} \mu_{\text{red}}^{(S,a)} v^{6j-2} \quad (32a)$$

$${}^{(2j+1)}\mu_{\text{bin}}^{aS} = \frac{(-)^j w}{(Gm)^{2j}} \mu_{\text{red}}^{(S,a)} v^{6j} \quad (32b)$$

where we have rewritten $\mathbf{x}_{12} = r_{12} \mathbf{n}_{12} = Gm v^{-2} \mathbf{n}_{12}$ in order to make all of the velocity dependence explicit. Each additional time derivative increases the pN order by 1.5 (i.e. it introduces three powers of v). Naturally here we are interested in either $2j$ or $2j+1$ being equal to $w = \ell_{\text{rad}} = 1 + \ell_1$, dependent on whether ℓ_1 is even or odd, which we expect to be the same parity as $|\epsilon|$ (see Sec. IV). Thus for $|\epsilon| = 0$ we expect to use Eq. (32b) with $2j = \ell_1 = s$, whereas for $|\epsilon| = 1$ we expect to use Eq. (32a) with $2j = 1 + \ell_1 = 1 + s$. This gives

$${}^{(w)}\mu_{\text{bin}}^{aS} = \frac{w}{(Gm)^s} \begin{cases} (-)^{(1+s)/2} \mu_{\text{red}}^{(S,a)} v^{3s+1}, & |\epsilon| = 1 \\ (-)^{s/2} \mu_{\text{red}}^{(S,a)} v^{3s}, & |\epsilon| = 0 \end{cases} \quad (33)$$

where we are still specializing to the case of $\ell_{\text{rad}} = w = 1 + s = 1 + \ell_1$.

IV. ESTIMATES OF MULTIPOLE MOMENTS

For this parameterization of theories, we can make scaling estimates of the multipole moments of bodies. This is straightforward for weakly gravitating bodies where the post-Newtonian approximation holds even in the interior of the body. It is not strictly true for strongly gravitating bodies, i.e. NSs or BHs, but we will boldly extrapolate on the principle of continuity.

A. Estimates: Isolated stationary compact objects

The interaction Lagrangian \mathcal{L}_{int} in Eq. (7) gives rise to a source term written schematically as

$$\tau \sim (m_{\text{pl}} \ell)^\varrho T[g, \epsilon^{0,1}, \nabla^d, R^r]. \quad (34)$$

This will enter into the source moments

$$\mu^Q = \int \tau x^Q d^3x = (m_{\text{pl}} \ell)^\varrho \int T[g, \epsilon^{0,1}, \nabla^d, R^r] x^Q d^3x. \quad (35)$$

Since exactly zero or one epsilon tensors may appear (see footnote 2), we will treat the even (zero epsilons) and odd (one epsilon) cases separately. As we shall see, these estimates suggest that even theories give rise just to even scalar multipole moments, and odd theories give rise just to odd scalar multipole moments.

1. Even sources: zero epsilons tensors

We make the following estimates: each curvature tensor will go as the density $G\rho$, and each derivative will introduce a power of R_*^{-1} where R_* is the radius of the star, which we further approximate as approximately spherical. This gives

$$\mu^Q \sim (m_{\text{pl}} \ell)^\varrho \frac{1}{R_*^d} \int (G\rho)^r r^q n^Q d\Omega r^2 dr. \quad (36)$$

The angular integration can be performed with the identity [14]

$$\int n^Q d\Omega = \begin{cases} \frac{4\pi}{q+1} \delta^{(Q)} & q \text{ even} \\ 0 & q \text{ odd} \end{cases} \quad (37)$$

where $\delta^{(Q)} = \delta^{(k_1 k_2 \dots k_{q-1} k_q)}$, an isotropic tensor. Here we see that only even q 's are sourced. Continuing with q even, and dropping the tensorial structure, we have

$$\mu^Q \sim (m_{\text{pl}} \ell)^\varrho \frac{1}{R_*^d} (G\rho_0)^r R_*^{q+3} \int_0^1 f^r u^{q+2} du \quad (38)$$

where $f = \rho/\rho_0$ is the dimensionless density profile with ρ_0 the central density, and $u = r/R_*$ is the dimensionless radius throughout the star. The final integral is dimensionless and though it contains information about how centrally concentrated the density profile is, we will drop it. Further, we will approximate $\rho_0 \approx M_*/R_*^3$ and take the compactness as $C_* = GM_*/R_*$. This gives

$$\mu^Q \sim (m_{\text{pl}} \ell) \left(\frac{\ell}{R_*}\right)^\varrho C_*^r R_*^q. \quad (39)$$

For black holes, we will replace R_* with GM_* and hence take the compactness C_* to be 1. Then we will have

$$\mu^Q \sim (m_{\text{pl}} \ell) \left(\frac{\ell}{GM_*}\right)^\varrho (GM_*)^q. \quad (40)$$

Consider for an example the case of EDGB where $d = 0$, $r = 2$, and the lowest non-vanishing BH moment is $\ell_{\text{BH}} = 0$, a “scalar charge.” We find

$$\mu_{\text{EDGB}} \sim (m_{\text{pl}}\ell) \frac{\ell}{GM_*}, \quad (41)$$

in agreement with the scaling found in [17] once we identify $m_{\text{pl}}\ell^2 \sim \alpha_3/\beta$.

2. Odd sources: one epsilon tensor

For the odd case, we will have one curvature tensor contribute dominantly the mass current $G\rho v^i$, while the remaining $r - 1$ curvature tensors dominantly contribute simply a mass density $G\rho$. We will assume the star undergoes solid body rotation about axis \hat{S}^i , so that the rotational velocity within the star can be written as

$$v^i = {}^{(3)}\epsilon^i{}_{jk}\hat{S}^j n^k v_{\text{eq}} \quad (42)$$

where again $u = r/R_*$ and v_{eq} is the rotational velocity at the surface at the equator. Inserting these approximations into the integral we have

$$\mu^Q \sim (m_{\text{pl}}\ell) \ell^\wp \frac{1}{R_*^d} \int \epsilon G\rho v (G\rho)^{r-1} x^Q d^3x \quad (43)$$

$$\sim (m_{\text{pl}}\ell) \ell^\wp \frac{1}{R_*^d} (G\rho_0)^r R_*^{q+3} \int \hat{S}^a v_{\text{eq}} u^{q+3} n^a d\Omega du \quad (44)$$

$$\mu^Q \sim v_{\text{eq}} \hat{S}^i (m_{\text{pl}}\ell) \left(\frac{\ell}{R_*}\right)^\wp C_*^r R_*^q. \quad (45)$$

As mentioned earlier, the integral in Eq. (44) is only non-vanishing for q odd. From here forward we drop the tensor structure.

Often times we may want this in terms of the dimensional spin angular momentum of the body used in relativity,³ S^i , with $[S^i] = [L]^2$ and $S^i \sim \hat{S}^i v_{\text{eq}} C_* R_*^2$. The above is rewritten as

$$\mu^Q \sim S(m_{\text{pl}}\ell) \left(\frac{\ell}{R_*}\right)^\wp C_*^{r-1} R_*^{q-2}. \quad (46)$$

Again for black holes we can replace R_* with GM_* and take the compactness to be 1, giving

$$\mu^Q \sim S(m_{\text{pl}}\ell) \left(\frac{\ell}{GM_*}\right)^\wp (GM_*)^{q-2}. \quad (47)$$

³ In geometric units, where $[M] = [L]$, spin angular momentum ($\mathbf{S}_{\text{geom}} = \int \mathbf{r} \times \mathbf{v} dm$) has dimensions of $[L]^2$, but in the units in this paper this definition would be dimensionless (i.e. angular momentum in units of \hbar , not appropriate for astrophysics). To convert to the usual relativists’ convention, we include a factor of G , $\mathbf{S} = G\mathbf{S}_{\text{geom}}$. This gives the scaling above.

As an example, consider dynamical Chern-Simons, where we have $d = 0$, $r = 2$, and the lowest non-vanishing BH moment is $\ell_{\text{BH}} = 1$, a scalar dipole moment. We have

$$\mu_{\text{CS}}^i \sim (m_{\text{pl}}\ell) \ell \frac{S^i}{(GM_*)^2} \quad (48)$$

which agrees with the scaling found in [18] once we identify $m_{\text{pl}}\ell^2 \sim \alpha/\beta$.

B. Estimates: Binary multipoles

We may estimate the scaling of μ_{red}^S (and therefore, for the case of $w = \ell_{\text{rad}} = 1 + s$, also ${}^{(w)}\mu_{\text{bin}}^{aS}$) by using the compact object scaling found above in Sec. IV A. For simplicity we will only examine the $|\epsilon| = 0$ case. Inserting Eq. (39) into Eq. (28), we have

$$\mu_{\text{red}}^S \sim \left[\frac{m_2}{m} (m_{\text{pl}}\ell) \left(\frac{\ell}{R_1}\right)^\wp C_1^r R_1^s - (1 \leftrightarrow 2) \right] \quad (49)$$

$$\mu_{\text{red}}^S \sim \frac{m_{\text{pl}}\ell\ell^\wp}{m} [m_2 (Gm_1)^{s-\wp} C_1^{\wp+r-s} - (1 \leftrightarrow 2)]. \quad (50)$$

Now we will take $C_A \sim \mathcal{O}(1)$. This expression is controlled by the difference $s - \wp$. Though we do not give a general expression, we can give the scaling for several small integer values of $s - \wp$. Specifically, we give the scalings for values of $s - \wp = -1, 0, +1, +2$ as follows:

$$\mu_{\text{red}}^S \sim (m_{\text{pl}}\ell) \ell^s \frac{\ell}{G\mu} \frac{\delta m}{m} \quad (s - \wp = -1) \quad (51a)$$

$$\mu_{\text{red}}^S \sim (m_{\text{pl}}\ell) \ell^s \frac{\delta m}{m} \quad (s - \wp = 0) \quad (51b)$$

$$\mu_{\text{red}}^S \sim (m_{\text{pl}}\ell) \ell^s \frac{G\mu}{\ell} \quad (s - \wp = +1) \quad (51c)$$

$$\mu_{\text{red}}^S \sim (m_{\text{pl}}\ell) \ell^s \frac{G\mu}{\ell} \frac{G\delta m}{\ell} \quad (s - \wp = +2) \quad (51d)$$

where $\delta m = m_1 - m_2$ and $\mu = m_1 m_2 / m$ is the reduced mass. As examples, dCS has $s - \wp = 0$, whereas in EDGB, for BHs we have $s - \wp = -1$, and for NSs we expect $s - \wp = +1$.

C. Regime of validity

Using these estimates of the multipole moments of compact objects, we can estimate the regime of validity of this present analysis. In order for our analysis to be valid, the correction due to the interaction term Eq. (7) must be small compared to the Einstein-Hilbert term Eq. (2). At the same time, if the correction starts to become large then there may be other higher-order interactions which should have also been included that would contribute.

A simple way to estimate the regime of validity of the theory is to analyze the ratio of the interaction Lagrangian to the Einstein-Hilbert Lagrangian,

$$\chi \equiv \frac{(m_{\text{pl}}\ell) \ell^\wp \theta T[g, \epsilon^{0,1}, \nabla^d, R^r]}{\frac{1}{2} m_{\text{pl}}^2 R}. \quad (52)$$

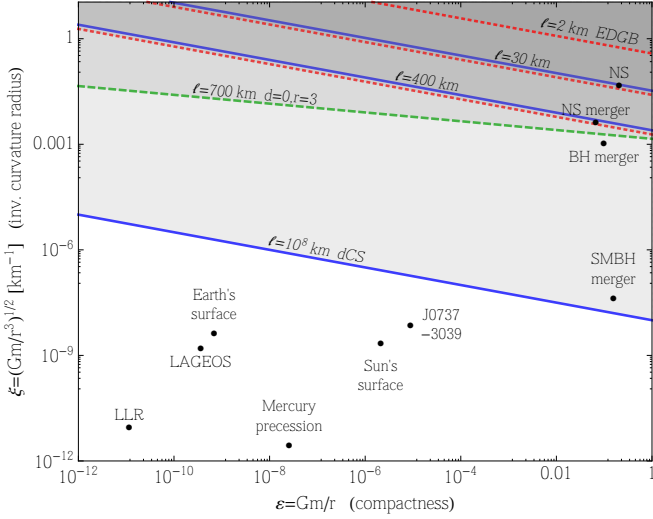


FIG. 1. (Color online) Regime of validity (small corrections) and invalidity (large corrections) of example theories with different values of ℓ . The shaded region (above the separating line) is the large-correction regime. The solid (blue online) curves correspond to dCS, while the dotted (red online) curves correspond to EDGB. As these two theories have the same d and r parameters, their lines have the same slopes [see Eq. (56)]. The dashed (green online) curve corresponds to some cubic-in-curvature interaction term. The vertical axis at left is the inverse curvature radius $\xi = (Gm/r^3)^{1/2}$ in units of km^{-1} . Larger values of ξ are stronger fields. The horizontal axis gives the dimensionless compactness $\varepsilon = (Gm/r)$ of a gravitating system. Larger values of ε are also stronger fields. Overplotted are various systems which have been (or will be) used as tests of gravity.

We use the scaling for θ , from Eq. (14), Eq. (39), and taking $r \sim R_*$,

$$\begin{aligned} \theta &\sim (2s-1)!! \frac{|\mu^S|}{r^{s+1}} \\ \theta &\sim (2s-1)!! (m_{\text{pl}} \ell) \left(\frac{\ell}{R_*} \right)^\varrho C_*^r R_*^{-1}. \end{aligned} \quad (53)$$

Inserting this and taking $\nabla \rightarrow R_*^{-1}$, $R \rightarrow G\rho$ gives

$$\chi \sim \frac{(2s-1)!! (m_{\text{pl}} \ell)^2 (\ell/R_*)^\varrho \ell^\varrho C_*^r R_*^{-d-1} (G\rho)^r}{\rho} \quad (54)$$

and after taking $\rho \sim M_*/R_*^3$ and a bit of simplification,

$$\chi \sim (2s-1)!! \left(\frac{\ell}{R_*} \right)^{2\varrho+2} C_*^{2r-1}. \quad (55)$$

Where this ratio is order unity, $\chi \sim 1$, separates the regime where corrections are small from the regime where corrections are order unity or larger.

In Fig. 1 we relate these regimes of validity or invalidity in a space of compactness vs. curvature radius, a choice of parameterization of the space of gravitational

phenomena.⁴ On the horizontal axis we have the dimensionless quantity $\varepsilon \equiv Gm/r$ where r stands for a typical length scale of some system, e.g. orbital radius of a binary or the radius of a neutron star. Larger ε is considered deeper into the strong-field regime. On the vertical axis we have inverse curvature radius $\xi = (Gm/r^3)^{1/2}$, with dimensions of km^{-1} . Larger values of ξ are also considered stronger fields. For reference we have plotted several gravitational systems which have been used as tests of gravity in the past or may be used as such in the future. Some examples of these systems are lunar laser ranging (LLR), the LAGEOS satellite, the perihelion precession of Mercury, the binary pulsar system J0737-3039, and the merger of two neutron stars and/or black holes.

To relate χ as given in Eq. (55) to this plane, we can take $C_* \rightarrow \varepsilon$, and $\xi = \sqrt{C_*}/R_*$ so $R_* \rightarrow \sqrt{\varepsilon}/\xi$. This means that the separatrix between small and large corrections is given on this plane as

$$1 \sim (2s-1)!! \varepsilon^{1-d} (\ell \xi)^{2\varrho+2} \quad (56)$$

for a given d, r , and s at a fixed ℓ .

We plot some examples of separatrices in Fig. 1. For both EDGB and dCS we have $d=0, r=2$ but we use $s=1$ for dCS and $s=2$ for EDGB. We have plotted a curve for each theory with both $\ell=30\text{km}$ (so the separatrix goes roughly through the NS surface point) and $\ell=400\text{km}$ (so the separatrix goes roughly through the NS-NS merger endpoint). The shaded region (above each line) is the large-correction regime, where our analysis is invalid, while the unshaded region (below each line) is the small-correction regime where the analysis is valid. These numbers should be compared to the present bounds. From Solar system experiments, ref. [19] estimated a bound on $\ell_{\text{dCS}} \lesssim 10^8\text{km}$. Meanwhile, from low-mass X-ray binaries ref. [20] estimated a bound on $\ell_{\text{EDGB}} \lesssim 1.9\text{km}$. The lines with the present bounds should be interpreted as follows: the small-correction regime is at least as large as the unshaded region shown for each theory, and the strong-correction regime may be any amount smaller than the shaded region shown.

From Fig. 1 it is easy to see why compact binary systems are a good candidate for testing strong-field corrections to GR. The top-right corner of this space is generically modified, while the Solar system and even many binaries are very weakly modified. NS-NS and stellar mass BH-BH binaries are the dynamical systems that make it deepest into the strong-field regime (an isolated NS is also deep in this regime but is not dynamical).

⁴ This is related to the energy (E) vs. occupation number (N) characterization more common in EFT. These may be related to more geometric quantities and to each other via $|\text{Riem}|^2 \sim \xi^4 \sim NE^6/m_{\text{pl}}^2$ and $|\nabla \text{Riem}|^2 \sim \xi^6/\varepsilon \sim NE^8/m_{\text{pl}}^2$.

V. SCALAR INTERACTION

The presence of scalar “hair” or “charge” for macroscopic gravitating bodies leads to a scalar interaction between the field generated by the body and an external field. This interaction in turn leads to several effects, among them an additional force on a body, a change in the binding energy of a compact binary system, and additional precession of pericenter of a compact binary system. The simplest approach to computing these effects is to work through an effective point-particle-with-hair Lagrangian, which is derived by “integrating out” the scalar field. In Sec. V A we integrate out the scalar field for an isolated body in an external scalar field, and find the scalar force on a body. In Sec. V B we integrate out the scalar field for a compact binary system to find the pole-pole interaction, and find the additional force. This allows for the computation of the additional pericenter precession (in Sec. VI).

A. General case

Consider an isolated compact object with charge μ_*^S giving rise to θ_* in the weak-field, and superpose an external scalar field θ_{ext} , $\theta = \theta_* + \theta_{\text{ext}}$. The Lagrangian for the canonical kinetic term, from Eq. (3), becomes

$$\mathcal{L}_{\text{kin}} = \mathcal{L}_{\text{self}} + \mathcal{L}_{\times} + \mathcal{L}_{\text{ext}} \quad (57)$$

with

$$\mathcal{L}_{\text{self}} = -\frac{1}{2}(\partial_a \theta_*)(\partial^a \theta_*) \quad (58)$$

$$\mathcal{L}_{\times} = -(\partial_a \theta_*)(\partial^a \theta_{\text{ext}}) \quad (59)$$

$$\mathcal{L}_{\text{ext}} = -\frac{1}{2}(\partial_a \theta_{\text{ext}})(\partial^a \theta_{\text{ext}}) \quad (60)$$

where \mathcal{L}_{\times} is the cross term between the field generated by the body and the external field, and is responsible for the force.⁵ Inserting the isolated WF solution [Eq. (14)] and integrating,

$$L_{\times}[\mathbf{x}_*] = \int \mathcal{L}_{\times} d^3x \quad (61)$$

$$= - \int \mu_*^S \left(\partial_{aS} \frac{1}{r_*} \right) (\partial^a \theta_{\text{ext}}) d^3x \quad (62)$$

$$L_{\times}[\mathbf{x}_*] = \int (-)^s \mu_*^S \left(\partial^a \partial_a \frac{1}{r_*} \right) (\partial_S \theta_{\text{ext}}) d^3x. \quad (63)$$

Now with the identity

$$\nabla^2 \frac{1}{r} = -4\pi \delta^3(\mathbf{x}) \quad (64)$$

⁵ The self-term is divergent (it vanishes under regularization [21]), but only the cross term contributes to the variation with respect to the location of the body, so the self-term may be dropped.

we easily find

$$L_{\times}[\mathbf{x}_*] = (-)^{s+1} 4\pi \mu_*^S (\partial_S \theta_{\text{ext}})[\mathbf{x}_*] \quad (65)$$

where the derivatives of θ_{ext} are evaluated at the location \mathbf{x}_* . The effective interaction Lagrangian can be treated as the negative of an interaction potential. The force on the body can be found as minus the “particle derivative” $[\partial_i^{(*)}]$ of the potential (i.e. differentiating with respect to the location of the particle) [11]. We find

$$F_*^i = \partial_i^{(*)} L_{\times}[\mathbf{x}_*] \quad (66)$$

$$F_*^i = (-)^s 4\pi \mu_*^S (\partial_{iS} \theta_{\text{ext}})[\mathbf{x}_*] \quad (67)$$

where the extra sign change comes from $\partial_i^{(*)} = -\partial_i$.

B. Compact binary multipole-multipole interaction

We now focus on the scalar interaction in a compact binary system with particles labeled by $A = 1, 2$, having lowest non-vanishing scalar multipole moments μ_1^S and μ_2^T with $s = |S| = \ell_1$ and $t = |T| = \ell_2$ (though the calculation holds for all moments, not just the lowest ones). Again we take the kinetic term, now inserting $\theta = \theta_1 + \theta_2$ the superposition of the two bodies’ multipolar fields. As before, we have three terms,

$$\mathcal{L}_{\text{kin}} = \mathcal{L}_{\text{self-1}} + \mathcal{L}_{\times} + \mathcal{L}_{\text{self-2}} \quad (68)$$

with

$$\mathcal{L}_{\text{self-1}} = -\frac{1}{2}(\partial_a \theta_1)(\partial^a \theta_1) \quad (69)$$

$$\mathcal{L}_{\times} = -(\partial_a \theta_1)(\partial^a \theta_2) \quad (70)$$

$$\mathcal{L}_{\text{self-2}} = -\frac{1}{2}(\partial_a \theta_2)(\partial^a \theta_2). \quad (71)$$

As before, only the cross term contributes to the pole-pole interaction. Inserting the isolated body WF solution [Eq. (14)] into the cross term, we have

$$L_{\times}[\mathbf{x}_1, \mathbf{x}_2] = - \int \mu_1^S \left(\partial_{aS} \frac{1}{r_1} \right) \mu_2^T \left(\partial^a \frac{1}{r_2} \right) d^3x. \quad (72)$$

Here we may integrate by parts to form either expression

$$L_{\times}[\mathbf{x}_1, \mathbf{x}_2] = (-)^{s+1} 4\pi \mu_1^S \mu_2^T \left(\partial_{ST} \frac{1}{r_2} \right) [\mathbf{x}_1] \quad (73)$$

$$= (-)^{t+1} 4\pi \mu_1^S \mu_2^T \left(\partial_{ST} \frac{1}{r_1} \right) [\mathbf{x}_2]. \quad (74)$$

This may also be written as

$$L_{\times}[\mathbf{x}_1, \mathbf{x}_2] = (-)^{t+1} 4\pi (2s + 2t - 1)!! \frac{\mu_1^S \mu_2^T n_{12}^{<ST>}}{r_{12}^{1+s+t}}. \quad (75)$$

This may not look symmetric under exchange of particle labels. However recall that under $1 \leftrightarrow 2$, we have

$n_{12} \rightarrow -n_{12}$, so the above transforms $(-)^{s+1}n_{12}^{<ST>} \rightarrow (-)^{t+1}n_{12}^{<ST>}$, hence the above expression is indeed symmetric under exchange of particle labels.

From this interaction Lagrangian we may find the conservative shift in the binding energy of a binary. As Eq. (75) contains no derivatives it's clear that when performing the Legendre transform to construct the Hamiltonian, $L_{\times}[\mathbf{x}_1, \mathbf{x}_2]$ will act just as a potential. Thus we immediately see

$$\delta E_{\text{bind}} = -L_{\times}[\mathbf{x}_1, \mathbf{x}_2] \quad (76)$$

$$\delta E_{\text{bind}} = (-)^t 4\pi(2s + 2t - 1)!! \frac{\mu_1^S \mu_2^T n_{12}^{<ST>}}{r_{12}^{1+s+t}}. \quad (77)$$

It is important to note here that when $s = 0 = t$, for example in the case of Brans-Dicke theory, this interaction term has the same radial dependence as the Kepler interaction term, $L_{\text{Kep}} = -Gm_1 m_2 / r_{12}$. This suggests that the $s = 0 = t$ case can be cast as a renormalization of Newton's constant. This one case is qualitatively different from all other possible values of $s + t$ and must be treated separately.

We may now compute $F_1^i = \partial_i^{(1)} L_{\times}$,

$$F_1^i = (-)^t 4\pi(2s + 2t + 1)!! \frac{\mu_1^S \mu_2^T n_{12}^{<iST>}}{r_{12}^{2+s+t}}. \quad (78)$$

The same calculation for F_2^i shows easily that $F_2^i = -F_1^i$.

VI. COMPACT BINARY PERICENTER PRESSION

We will now compute the primary observable for a compact binary pulsar under this conservative correction, the precession of the pericenter of the binary, $\langle \dot{\omega} \rangle$. This calculation usually comes with the rate of change of eccentricity \dot{e} , rate of change of semi-major axis \dot{a} , rate of change of inclination $\frac{d}{dt} \iota$, and rate of change of angle of the ascending node $\dot{\Omega}$. We will only compute $\dot{\omega}$.

We follow Gauss' perturbation method [1, 22, 23] with the conventions and notation of [1]. One must then calculate the relative perturbing acceleration δa_{12}^i (in any convenient coordinate system). This vector is then decomposed by projecting onto a *time-varying* orthonormal triad with $e_1^i = n_{12}^i$ and $e_2^i = \hat{L}^i$ (and $e_3 = e_2 \times e_1$ so as to complete the orthonormal triad). In this triad, the components of δa_{12}^i are defined as [1]

$$\mathcal{R} \equiv \delta a_{12}^i e_{1,i}, \quad (79a)$$

$$\mathcal{W} \equiv \delta a_{12}^i e_{2,i}, \quad (79b)$$

$$\mathcal{S} \equiv \delta a_{12}^i e_{3,i}, \quad (79c)$$

where inner products are taken with a flat Euclidean metric. With this decomposition, the pericenter of the

osculating orbit evolves secularly as

$$\dot{\omega} = -\frac{p\mathcal{R}}{he} \cos \phi + \frac{(p+r)\mathcal{S}}{he} \sin \phi - \dot{\Omega} \cos \iota, \quad (80)$$

$$\dot{\Omega} = \frac{\mathcal{W}r}{h} \sin(\omega + \phi) \csc \iota. \quad (81)$$

Here,

$$p \equiv a(1 - e^2) \quad (82)$$

is the semi-latus rectum, r and ϕ are the quantities related to the instantaneous orbital elements, given by

$$r \equiv \frac{p}{1 + e \cos \phi}, \quad (83)$$

$$r^2 \frac{d\phi}{dt} \equiv h \equiv \sqrt{Gmp}, \quad (84)$$

where h is the orbital angular momentum per unit mass. In Eq. (80), the right-hand side is to be orbit averaged as any quantity Q ,

$$\langle Q \rangle = \frac{1}{T} \oint Q dt = \frac{1}{T} \int_0^{2\pi} \frac{Q(\phi) d\phi}{\dot{\phi}}, \quad (85)$$

where T is the background orbital period $T = 2\pi a^{3/2} / \sqrt{Gm}$, ϕ is the orbital phase, and the Jacobian $\dot{\phi}$ must of course be included [from Eq. (84)]. This procedure is appropriate when the time derivatives of the osculating elements are much smaller than the orbital timescale and there are no resonances. Of course, all of the ϕ dependence in $\mathcal{R}, \mathcal{W}, \mathcal{S}$ and r must be included in the orbit averaging. This procedure gives, for the leading GR pericenter precession,

$$\langle \dot{\omega} \rangle_{\text{GR}} = \frac{1}{T} \frac{6\pi Gm}{a(1 - e^2)} = \frac{3(Gm)^{3/2}}{(1 - e^2)a^{5/2}}. \quad (86)$$

With the pole-pole force in hand from Eq. (78) we can compute the relative acceleration,

$$a_{12}^i = a_1^i - a_2^i = \left(\frac{1}{m_1} + \frac{1}{m_2} \right) F_1^i = \frac{1}{\mu} F_1^i \quad (87)$$

where again the reduced mass is $\mu = m_1 m_2 / m$. This acceleration is decomposed as

$$\mathcal{R} = \mathcal{A} \mu_1^S \mu_2^T \times n_{12}^{<iST>} n_{12}^i (1 + e \cos \phi)^{2+s+t} \quad (88a)$$

$$\mathcal{S} = \mathcal{A} \mu_1^S \mu_2^T \hat{L}^i \times n_{12}^{<iST>} (1 + e \cos \phi)^{2+s+t} \quad (88b)$$

$$\mathcal{W} = \mathcal{A} \mu_1^S \mu_2^T \epsilon_{ijk} \hat{L}^j \times n_{12}^{<iST>} n_{12}^k (1 + e \cos \phi)^{2+s+t} \quad (88c)$$

with all of the ϕ dependence to the right of \times in each expression (remember that n_{12} rotates with the orbit), and where we have defined

$$\mathcal{A} \equiv \frac{1}{\mu} (-)^t 4\pi(2s + 2t + 1)!! p^{-(2+s+t)}. \quad (89)$$

These expressions are subject to the identities [15]

$$n_i n_{\langle a_1 \dots a_l \rangle} = n_{\langle i a_1 \dots a_l \rangle} + \frac{l}{2l+1} \delta_{i \langle a_1} n_{a_2 \dots a_l \rangle} \quad (90)$$

and by contracting,

$$n_i n_{\langle i L \rangle} = \frac{l+1}{2l+1} n_{\langle L \rangle}. \quad (91)$$

Inserting the decomposed acceleration [Eq. (88)] into the expression for $\dot{\omega}$ [Eq. (80)] and then orbit averaging [Eq. (85)] we arrive at

$$\langle \dot{\omega} \rangle = \frac{1}{T} \frac{p^2}{Gm} \mathcal{A} \mu_1^S \mu_2^T \left[-\frac{1}{e} \frac{s+t+1}{2s+2t+1} I_1^{ST} + \frac{1}{e} \hat{L}^i I_2^{iST} - \cot \iota \frac{s+t+1}{2s+2t+3} \epsilon_{ijk} \hat{L}^j I_3^{ikST} \right] \quad (92)$$

where we have defined the three tensor-valued integrals

$$I_1^{ST} = \int_0^{2\pi} n_{12}^{\langle ST \rangle} (1 + e \cos \phi)^{s+t} \cos \phi d\phi \quad (93a)$$

$$I_2^{iST} = \int_0^{2\pi} n_{12}^{\langle iST \rangle} (1 + e \cos \phi)^{s+t-1} (2 + e \cos \phi) \sin \phi d\phi \quad (93b)$$

$$I_3^{ikST} = \int_0^{2\pi} \delta^{k \langle i} n_{12}^{ST \rangle} (1 + e \cos \phi)^{s+t-1} \sin(\omega + \phi) d\phi \quad (93c)$$

which are all functions of eccentricity of order unity.

Here we can immediately extract the relative pN order of this effect. Recalling that $T \propto a^{3/2}$, $p \propto a$, $\alpha \propto v^{-2}$, and $\mathcal{A} \propto p^{-(2+s+t)}$, we have

$$\langle \dot{\omega} \rangle \propto v^{2(s+t)+3} \quad (94)$$

$$\frac{\langle \dot{\omega} \rangle}{\langle \dot{\omega} \rangle_{\text{GR}}} \propto v^{2(s+t-1)}. \quad (95)$$

We will go into more detail in the next subsection. We remind the reader here that for the special case of $s = 0 = t$, the pole-pole interaction term can be absorbed by a rescaling of Newton's constant, so it is not actually

pre-Newtonian. For other values of s, t , only the sum $s + t$ enters this scaling, and the pericenter precession is of relative $+(s + t - 1)$ pN order. Remember that s, t should have the same parity, so $s + t$ is even, and therefore this effect is always of odd relative pN order, starting at relative $+1$ pN.

A. Pericenter precession scaling estimates

In order to estimate the bounds which may be placed on ℓ in a given theory, we must study how the ratio $\langle \dot{\omega} \rangle / \langle \dot{\omega} \rangle_{\text{GR}}$ scales with ℓ , \wp , the constituent masses, radii, scalar multipole moments, and orbital velocity.

The dependence on ℓ is buried inside the scaling of the multipole tensors μ_A^Q where $A = 1, 2$ and $|Q| = s, t$ for respectively bodies 1, 2. We here repeat the scaling found in Sec. IV A for $|\epsilon| = 0$ (for $|\epsilon| = 1$, the quantity v_{eq} must also be included). We found

$$\mu^Q \sim (m_{\text{pl}} \ell) \left(\frac{\ell}{R_*} \right)^\wp C_*^r R_*^q$$

for a body with radius R_* and compactness C_* . This we insert into Eq. (92). At the same time, we also pull the eccentricity dependence (in $I_{1,2,3}$) into a function $f_1(e)$ which is of order unity. This gives

$$\langle \dot{\omega} \rangle \sim (-)^t (2s + 2t + 1)!! \frac{1}{T} \frac{\ell^2}{(Gm)(G\mu)} \left(\frac{\ell^2}{R_1 R_2} \right)^\wp \times (C_1 C_2)^r \left(\frac{R_1}{p} \right)^s \left(\frac{R_2}{p} \right)^t f_1(e) \quad (96)$$

where R_A and C_A with $A = 1, 2$ are respectively the radius and compactness of body A . We compare $\langle \dot{\omega} \rangle$ to the GR expression in Eq. (86) by taking their ratio. There is yet more eccentricity dependence in $p = a(1 - e^2)$ [from Eq. (82)] which we absorb into a new function $f_2(e)$ which is also of order unity. We will also remove all of the dependence on the semi-major axis a in favor of the orbital velocity through the Kepler relation $v^2 = Gm/a$. This gives

$$\frac{\langle \dot{\omega} \rangle}{\langle \dot{\omega} \rangle_{\text{GR}}} \sim (-)^t (2s + 2t + 1)!! \frac{\ell^2}{(Gm)(G\mu)} \left(\frac{\ell^2}{R_1 R_2} \right)^\wp (C_1 C_2)^r \left(\frac{R_1}{Gm} \right)^s \left(\frac{R_2}{Gm} \right)^t f_2(e) v^{2(s+t-1)}. \quad (97)$$

This result reproduces the dCS pericenter precession as calculated in Eq. (131) of [12]. However, we can not compare to the EDGB result: Again we have the caveat that for $s = t = 0$, the pole-pole interaction can be absorbed by rescaling G , so the modification is pushed to a higher order.

Finally, let us note an effect which we have not computed here. There will be metric deformations which also contribute to pericenter precession with the same dependence on ℓ as this scalar interaction effect. For example, in dCS the correction to the metric quadrupole-monopole interaction can dominate over the scalar dipole-dipole

interaction, depending on the spins of the two bodies [12].

VII. COMPACT BINARY RADIATION REACTION

In the dissipative sector of the dynamics, the binding energy (and angular momentum) of the binary is carried away by radiation in all dynamical fields. Both the metric and scalar contribute, as do any other additional degrees of freedom, but here we only consider the scalar field.

The energy flux in some field φ is quantified in the stress-energy tensor⁶ $T_{ab}^{(\varphi)}$. Specifically, the energy flux is calculated as the integral of the flux density over a 2-sphere approaching asymptotic infinity, captured in the component $T_{ti}^{(\varphi)} n^i$ where n^i is the outward unit normal. We have for such a field (see Sec. VI of [11])

$$\dot{E}^{(\varphi)} = \lim_{r \rightarrow \infty} \int_{S_r^2} \langle T_{ti}^{(\varphi)} n^i \rangle r^2 d\Omega, \quad (98)$$

where again $\langle \rangle$ is an orbit-averaged quantity.

For the scalar field with canonical kinetic term and flat potential, we have the stress-energy tensor

$$T_{ab}^{(\theta)} = (\partial_a \theta)(\partial_b \theta) - \frac{1}{2} g_{ab} (\partial \theta)^2. \quad (99)$$

Here we will insert the far-zone, radiative solution from Eq. (24), and use the identity [Eq. (22)] $\partial_i \theta = -n^i \partial_t \theta$ in

$$\dot{E}^{(\theta)} = -\frac{1}{(s!)^2} \frac{4\pi}{2w+1} \frac{1}{(Gm)^{2w}} \mu_{\text{red}}^S \mu_{\text{red}}^T \delta_{(abST)} \left\langle \begin{array}{l} n_{12}^a n_{12}^b v^{6s+8} \\ v_{12}^a v_{12}^b v^{6s+6} \end{array} \right\rangle, \quad \begin{array}{l} |\epsilon| = 0 \\ |\epsilon| = 1 \end{array} \quad (103)$$

where $|S| = s = |T|$ and where we have taken μ_{red} to be constant over the timescale of an orbit. Again remember that this is for the case of $w = 1 + s$.

This is to be compared with the gravitational wave luminosity in GR, which in the circular limit is given by the well-known expression

$$\dot{E}^{\text{GW}} = -\frac{32}{5} G \mu^2 r_{12}^4 \omega^6 = -\frac{32}{5} \frac{1}{G} \frac{\mu^2}{m^2} v^{10}, \quad (104)$$

where in the second equality, we have used the Kepler relation. From this we see that the scalar flux $\dot{E}^{(\theta)}$ is of relative $+(3s-1)$ pN order compared to the gravitational wave flux.

the far zone. Combining, we have

$$T_{ti}^{(\theta)} n^i = -(\partial_t \theta)^2 = -\frac{1}{r^2} \frac{1}{(w!)^2} \left[n_W^{(w+1)} \mu_{\text{bin}}^W \right]^2 \quad (100)$$

where $w = |W| = \ell_{\text{rad}}$. The quantity μ_{bin} has no dependence on n^i , being defined in the NZ. Therefore the angular integral can be performed, with the aid of Eq. (37), giving

$$\dot{E}^{(\theta)} = -\frac{1}{(w!)^2} \frac{4\pi}{2w+1} \delta_{(VW)} \left\langle n_W^{(w+1)} \mu_{\text{bin}}^V \mu_{\text{bin}}^W \right\rangle \quad (101)$$

where $|V| = w = |W|$ with $V = a_1 \cdots a_w$, $W = b_1 \cdots b_w$, and $\delta_{(VW)} = \delta_{(a_1 b_1 \cdots a_w b_w)}$.

Now we use the calculation of an arbitrary number of derivatives of μ_{bin}^{aS} , given in Eqs. (32). Notice that $1 + w = 2 + s$ has the same parity as s . For $|\epsilon| = 0$, s is even and we will take an even number of derivatives, using Eq. (32a) with $2j = 1 + w$, whereas for $|\epsilon| = 1$ we will have s odd, take an odd number of derivatives, and therefore use Eq. (32b) with $2j = w$. This gives

$$\mu_{\text{bin}}^{aS} = \frac{w}{(Gm)^w} \begin{cases} (-)^{(2+s)/2} \mu_{\text{red}}^S n_{12}^a v^{3s+4}, & |\epsilon| = 0 \\ (-)^{(1+s)/2} \mu_{\text{red}}^S v_{12}^a v^{3s+3}, & |\epsilon| = 1 \end{cases} \quad (102)$$

Combining, we find

A. Radiation reaction scaling estimates

By using the scaling estimates given in Sec. IV B, we can estimate the scaling of the extra energy lost from the binary due to scalar radiation. We are interested in the (small) ratio $\dot{E}^{(\theta)}/\dot{E}^{\text{GW}}$, for the total energy loss is $\dot{E} = \dot{E}^{\text{GW}}(1 + \dot{E}^{(\theta)}/\dot{E}^{\text{GW}})$. The flux ratio is proportional to a power of ℓ through μ_{red} .

For simplicity we will only consider $|\epsilon| = 0$. Combining Eq. (103) and Eq. (104), after a small amount of algebra, we have

$$\frac{\dot{E}^{(\theta)}}{\dot{E}^{\text{GW}}} \sim \frac{5\pi^2}{(2w+1)(s!)^2} \frac{m_{\text{pl}}^2}{\mu^2} \frac{|\mu_{\text{red}}^S|^2}{(Gm)^{2s}} v^{6s-2}. \quad (105)$$

Now we insert, for μ_{red}^S , the four scalings we found in Sec. IV B, given by the four differences $s - \wp$ =

⁶ Or, in the case of the metric, in the effective stress-energy tensor of gravitational waves [24].

$-1, 0, +1, +2$. We find, after a bit of simplification,

$$\frac{\dot{E}^{(\theta)}}{\dot{E}^{\text{GW}}} \sim \frac{\eta^{-4} v^{6s-2}}{(2w+1)(s!)^2} \left(\frac{\ell}{Gm}\right)^{2+2\wp} \frac{\delta m^2}{m^2} \quad (s - \wp = -1) \quad (106a)$$

$$\frac{\dot{E}^{(\theta)}}{\dot{E}^{\text{GW}}} \sim \frac{\eta^{-2} v^{6s-2}}{(2w+1)(s!)^2} \left(\frac{\ell}{Gm}\right)^{2+2\wp} \frac{\delta m^2}{m^2} \quad (s - \wp = 0) \quad (106b)$$

$$\frac{\dot{E}^{(\theta)}}{\dot{E}^{\text{GW}}} \sim \frac{v^{6s-2}}{(2w+1)(s!)^2} \left(\frac{\ell}{Gm}\right)^{2+2\wp} \quad (s - \wp = +1) \quad (106c)$$

$$\frac{\dot{E}^{(\theta)}}{\dot{E}^{\text{GW}}} \sim \frac{v^{6s-2}}{(2w+1)(s!)^2} \left(\frac{\ell}{Gm}\right)^{2+2\wp} \frac{\delta m^2}{m^2} \quad (s - \wp = +2) \quad (106d)$$

where $\eta = m_1 m_2 / m^2 = \mu / m$. Some of these expressions reproduce results published previously in the literature, while others are new. For EDGB with two BHs, we have $s - \wp = -1$, given in Eq. (106a). This equation reproduces the same scaling with η , the ratio $(\delta m / m)$, and the relative post-Newtonian order as given by [11] in their Eq. (134). For dCS and either NSs or BHs, we have $s - \wp = 0$, given in Eq. (106b). This reproduces the scaling with η and the post-Newtonian order given by [11] in their Eq. (139) (though this comparison is not well justified, since here we have only estimated the scaling for $|\epsilon| = 0$ theories).

VIII. GRAVITATIONAL WAVE SIGNATURE

In this section, we derive a correction to the gravitational waveform phase (in the Fourier domain) of a compact binary system. We only show the scaling estimate and neglect numerical factors. For simplicity, we restrict our attention to binaries with a circular orbit, for the case of $s = t$, and with $|\epsilon| = 0$. In order to accomplish this goal, we need to combine three ingredients: corrections to i) the binding energy, ii) the Kepler relation, and iii) the energy flux. We then proceed through the stationary phase approximation (see e.g. [25]).

In Eq. (77), we derived a correction to the binding energy due to the pole-pole interaction. In general, there is also a correction to the binding energy due to the fact that the spacetime around the compact object is deformed, which we have not addressed in this paper. Let us parameterize this by

$$\delta E_{\text{bind}}^{\text{def}} = \frac{C_{\text{def}}}{r^{1+n_{\text{def}}}}, \quad (107)$$

where the coefficient C_{def} has units of $[C_{\text{def}}] = [L]^{n_{\text{def}}}$. Note that this deformation is of $+n_{\text{def}}$ pN order relative to GR. For example, $n_{\text{def}} = 2$ for both EDGB [17] and dCS [12, 26, 27]. By combining this with the force due to the pole-pole interaction shown in Eq. (78), we can derive

the equation of motion of a binary as

$$r_{12} \omega^2 \sim \frac{Gm}{r_{12}^2} \left[1 + \frac{1}{Gm\mu} \frac{|\mu_1 \mu_2|}{r^{2s}} + \frac{1}{Gm\mu} \frac{C_{\text{def}}}{r^{n_{\text{def}}}} \right]. \quad (108)$$

By assuming that the orbital velocity $v \sim (Gm\omega)^{1/3}$ is much less than the speed of light, we can invert the above expression by expanding in terms of v and obtain the modified Kepler relation $r_{12}(\omega)$ as

$$r_{12}(\omega) \sim \frac{Gm}{(Gm\omega)^{2/3}} \left[1 + \frac{1}{Gm\mu} \frac{|\mu_1 \mu_2|}{(Gm)^{2s}} (Gm\omega)^{4s/3} + \frac{1}{Gm\mu} \frac{C_{\text{def}}}{(Gm)^{n_{\text{def}}}} (Gm\omega)^{2n_{\text{def}}/3} \right]. \quad (109)$$

By using Eqs. (77), (107) and (109), we obtain the binding energy in terms of $(Gm\omega)$ as

$$E_{\text{bind}} \sim \mu (Gm\omega)^{2/3} \left[1 + \frac{1}{Gm\mu} \frac{|\mu_1 \mu_2|}{(Gm)^{2s}} (Gm\omega)^{4s/3} + \frac{1}{Gm\mu} \frac{C_{\text{def}}}{(Gm)^{n_{\text{def}}}} (Gm\omega)^{2n_{\text{def}}/3} \right]. \quad (110)$$

Next, we move onto the dissipative correction, namely the one to the energy flux. In Eq. (103), we derived the energy flux for the scalar radiation. There is also a correction to the energy flux for the gravitational radiation that we have not addressed in this paper. This we parameterize as

$$\dot{E}^{(h)} = C_h \left(\frac{Gm}{r_{12}} \right)^{5+n_h}, \quad (111)$$

where C_h has dimensions of $[C_h] = [L]^{-2}$. Notice that $\dot{E}^{(h)}$ gives an $+n_h$ pN correction relative to GR. For example, we have $n_h = 0$ for EDGB and $n_h = 2$ for dCS [11]. Combining with Eqs. (103) and (109), we find

$$\begin{aligned} \dot{E} \sim \frac{\eta^2}{G} (Gm\omega)^{10/3} & \left[1 + \frac{1}{Gm\mu} \frac{|\mu_1 \mu_2|}{(Gm)^{2s}} (Gm\omega)^{4s/3} \right. \\ & + \frac{1}{Gm\mu} \frac{C_{\text{def}}}{(Gm)^{n_{\text{def}}}} (Gm\omega)^{2n_{\text{def}}/3} \\ & + \frac{G}{\eta^2 (Gm)^2} \frac{|\mu_{\text{red}}|^2}{(Gm)^{2s}} (Gm\omega)^{2s-2/3} \\ & \left. + \frac{GC_h}{\eta^2} (Gm\omega)^{2n_h/3} \right]. \quad (112) \end{aligned}$$

One can obtain the gravitational waveform phase $\Psi(f)$ for the dominant harmonic in the Fourier domain from the relation [25]

$$\frac{d^2 \Psi}{d\omega^2} = 2 \frac{dE}{d\omega} \frac{dt}{dE}. \quad (113)$$

By substituting Eqs. (110) and (112) into the above equation and integrating, we obtain

$$\begin{aligned} \Psi(f) \sim & \frac{1}{\eta} (\pi G m f)^{-5/3} + \frac{1}{\eta^2 G m^2} \frac{|\mu_1 \mu_2|}{(Gm)^{2s}} (\pi G m f)^{(4s-5)/3} \\ & + \frac{1}{\eta^2 G m^2} \frac{C_{\text{def}}}{(Gm)^{n_{\text{def}}}} (\pi G m f)^{(2n_{\text{def}}-5)/3} \\ & + \frac{1}{\eta^3 G m^2} \frac{|\mu_{\text{red}}|^2}{(Gm)^{2s}} (\pi G m f)^{(6s-7)/3} \\ & + \frac{G C_h}{\eta^3} (\pi G m f)^{(2n_h-5)/3} \end{aligned} \quad (114)$$

for the dominant harmonic. The leading term corresponds to the leading GR gravitational-wave phase. Each of the four correction terms arises from a unique physical effect. We will number these effects as follows:

1. The correction proportional to $|\mu_1 \mu_2|$ comes from the scalar pole-pole interaction modifying the binding energy and Kepler relation.
2. The correction proportional to C_{def} comes from the metric deformation modifying the binding energy and Kepler relation.
3. The correction proportional to $|\mu_{\text{red}}|^2$ comes from the energy lost via scalar radiation.
4. The correction proportional to C_h comes from the correction to the gravitational wave energy flux.

In EDGB, correction 3 (scalar energy loss) dominates, giving a -1 pN correction relative to GR [11], while in dCS all the correction terms contribute at the same order, $+2$ pN relative to GR [12, 27].

A. Mapping to post-Einsteinian parameters

The gravitational waveform phase in alternative theories of gravity can be expressed using the so-called parameterized post-Einsteinian (ppE) waveform phase $\Psi_{\text{ppE}}(f)$ as [28]

$$\Psi_{\text{ppE}}(f) = \Psi_{\text{GR}}(f) + \beta_{\text{ppE}} (\pi G \mathcal{M} f)^{b_{\text{ppE}}}, \quad (115)$$

where $\mathcal{M} = m\eta^{3/5}$ is the chirp mass. The correction found in Eq. (114) can be mapped to the ppE waveform phase above.

The four corrections enumerated above correspond to:

$$b_{\text{ppE}}^{(1)} = (4s - 5)/3 \quad (116a)$$

$$b_{\text{ppE}}^{(2)} = (2n_{\text{def}} - 5)/3 \quad (116b)$$

$$b_{\text{ppE}}^{(3)} = (6s - 7)/3 \quad (116c)$$

$$b_{\text{ppE}}^{(4)} = (2n_h - 5)/3. \quad (116d)$$

We may also extract the β_{ppE} parameters from Eq. (114) after converting to \mathcal{M} . Each one of the four β 's should

be proportional to a power of ℓ . In this paper we have developed the scalings for corrections 1 and 3 (proportional to $|\mu_1 \mu_2|$ and $|\mu_{\text{red}}|^2$, respectively). For corrections 2 and 4 we can only go so far as to say

$$\beta_{\text{ppE}}^{(2)} \sim \frac{1}{\eta^{1+2n_{\text{def}}/5} G m^2} \frac{C_{\text{def}}}{(Gm)^{n_{\text{def}}}} \quad (117a)$$

$$\beta_{\text{ppE}}^{(4)} \sim \frac{G C_h}{\eta^{2+2n_h/5}}. \quad (117b)$$

For correction 1 we may go farther by using the scaling from Sec. IV A. For simplicity, we are focusing on the case with $s = t$, and $|\epsilon| = 0$. This gives

$$\beta_{\text{ppE}}^{(1)} \sim \frac{\ell^2}{\eta^{1+4s/5} (Gm)^2} \left(\frac{\ell^2}{R_1 R_2} \right)^{\wp} \left(\frac{R_1 R_2}{(Gm)^2} \right)^s (C_1 C_2)^r. \quad (117c)$$

Finally for correction 3 we may use the scaling estimates for μ_{red} from Sec. IV B. As we saw, the scaling of μ_{red} is controlled by the difference $s - \wp$, and we gave four examples in Eq. (51) for $s - \wp = -1, 0, +1, +2$. For these same four values we have

$$\beta_{\text{ppE}}^{(3)} \sim \frac{1}{\eta^{(12+6\wp)/5}} \left(\frac{\ell}{Gm} \right)^{2+2\wp} \left(\frac{\delta m}{m} \right)^2 \quad (s - \wp = -1) \quad (117d)$$

$$\beta_{\text{ppE}}^{(3)} \sim \frac{1}{\eta^{(8+6\wp)/5}} \left(\frac{\ell}{Gm} \right)^{2+2\wp} \left(\frac{\delta m}{m} \right)^2 \quad (s - \wp = 0) \quad (117e)$$

$$\beta_{\text{ppE}}^{(3)} \sim \frac{1}{\eta^{(4+6\wp)/5}} \left(\frac{\ell}{Gm} \right)^{2+2\wp} \quad (s - \wp = +1) \quad (117f)$$

$$\beta_{\text{ppE}}^{(3)} \sim \frac{1}{\eta^{(10+6\wp)/5}} \left(\frac{\ell}{Gm} \right)^{2+2\wp} \left(\frac{\delta m}{m} \right)^2. \quad (s - \wp = +2) \quad (117g)$$

We can compare these results with some already present in the literature. Reference [11] computed the correction due to effect 3 (scalar energy flux correction) for black hole binaries in both EDGB and dCS. For EDGB they found $b_{\text{ppE}} = -7/3$ and $\beta_{\text{ppE}} \sim \zeta_3 \eta^{-18/5} (\delta m/m)^2$. Here, from Eq. (116c) we find the same value of b_{ppE} . We use the $s - \wp = -1$ result [Eq. (117d)] which also agrees with the result of [11] once we make the identification of $\zeta_3 \sim (\ell/Gm)^4$ (this is in agreement with their definition of ζ_3 and our earlier identification of $\alpha_3 \sim m_{\text{p1}} \ell^2$).

For dCS, ref. [11] found $b_{\text{ppE}} = -1/3$ and $\beta_{\text{ppE}} \sim \zeta_4 \eta^{-14/5} \bar{\Delta}^2$ where their $\bar{\Delta} = \chi_1 \hat{\mathbf{S}}_1 m_2/m - (1 \leftrightarrow 2)$ is a dimensionless vector encoding some combination of the spins of the black holes (with $0 \leq \chi_A \leq 1$ the dimensionless spin of body A). This combination has the property that $\bar{\Delta}^2 \rightarrow (\delta m/m)^2$ in the limit of co-aligned maximal spins. While our analysis ignored spin (we only considered $|\epsilon| = 0$) we have agreement on b_{ppE} and the scaling of β_{ppE} with η . A more thorough analysis would capture the spin dependence in $\bar{\Delta}$, which at least gives the same $(\delta m/m)$ dependence we find in the co-aligned extremal

spin limit. Again we need to identify $\zeta_4 \sim (\ell/Gm)^4$ (and this again agrees with their definition of ζ_4 and our earlier identification of $\alpha_4 \sim m_{\text{pl}}\ell^2$).

IX. BOUNDS ESTIMATE

In this section we estimate the bounds that could be placed on ℓ , from measurements of pericenter precession in pulsar binaries (Sec. VI) and from gravitational wave measurements (Sec. VIII).

A. Pericenter precession bounds

We again consider a pulsar binary system. In order to bound ℓ in some given theory [with values given for $(|\epsilon|, d, r, \ell_{\text{NS}}, \ell_{\text{BH}})$] requires a high-quality timing solution with several pK (post-Keplerian) parameters well-constrained [29]. In this case the pericenter precession is measured within some variance $\sigma_{\langle\dot{\omega}\rangle}^2$ (and co-variant with other timing parameters, which we ignore here for simplicity). A proper constraint on ℓ would require forming more timing solutions with ℓ a free parameter, including the additional precession given in Eq. (92). However here we can make a simple estimate of the bounds which could be placed.

A simple estimate comes from ascribing all the variance σ^2 (we now drop the subscript) to the additional precession in Eq. (92). We combine this with the scaling estimate given in Eq. (97): change the left hand side to the ratio $|\sigma/\langle\dot{\omega}\rangle|$ and the scaling to an inequality. This can be solved, for a given theory's parameters and system's parameters, for a bound on ℓ . Specifically, we will have the scaling (now taking $s = t$)

$$\ell^{2+2\varphi} \lesssim \frac{|\sigma|}{\langle\dot{\omega}\rangle} \frac{GmG\mu R_1^{\varphi} R_2^{\varphi}}{(4s+1)!! C_1^r C_2^r} \left[\frac{(Gm)^2}{R_1 R_2} \right]^s v^{2(1-2s)}. \quad (118)$$

Some examples of such estimated bounds are plotted in Fig. 2. On the horizontal axis we have the dimensionless compactness of a pulsar binary system [related to the orbital velocity in Eq. (97) via the leading-order Kepler relation $v^2 = Gm/a = \epsilon$]. On the (right, inverted) vertical axis is the estimated bound on ℓ . Values of ℓ shorter than (therefore up in the plot) the plotted curves would be allowed, while values greater (therefore down in the plot) would be ruled out. The pericenter precession estimates appear as sloped lines—clearly, larger values of Gm/a would produce better constraints on ℓ .

The solid (blue online) curves correspond to the parameters of dCS while the dotted (red online) curves correspond to the parameters of EDGB. The lower curve of each pair corresponds to a value of $|\sigma/\langle\dot{\omega}\rangle| \sim 1$ while the upper curve of each pair corresponds to $|\sigma/\langle\dot{\omega}\rangle| \sim 10^{-2}$. Naturally a better measurement of $\langle\dot{\omega}\rangle$ leads to a better constraint on ℓ . To generate each curve we used a fiducial NS-NS system (so $s = t$) with masses $m_1 = 1.4M_{\odot} = m_2$

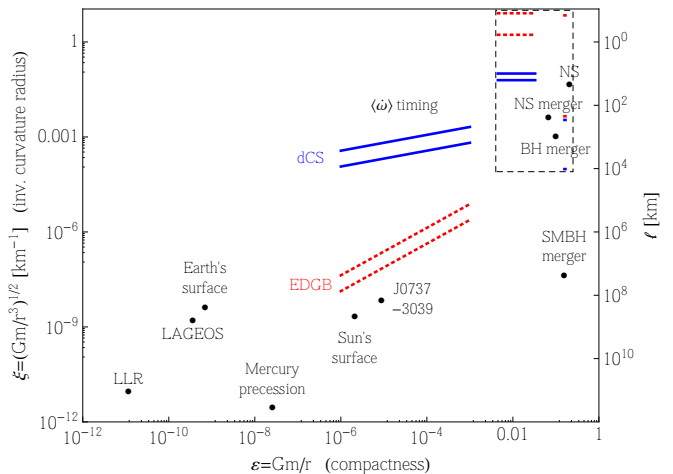


FIG. 2. (Color online) Estimated bounds on ℓ . Upward sloping curves are estimates from pericenter precession coming from Eq. (118). The vertical axis at right is the length scale ℓ of the bound. The horizontal axis gives the compactness (Gm/a) of a binary which yields a bound. Solid (blue online) curves correspond to bounds for dCS, while dotted (red online) curves correspond to EDGB. The lower curve for each theory is the estimate for $|\sigma/\langle\dot{\omega}\rangle| \sim 1$ while the upper curve is for $|\sigma/\langle\dot{\omega}\rangle| \sim 10^{-2}$. The dashed region is expanded in Fig. 3 to show estimated bounds from gravitational waves.

and radii $R_1 = 10\text{km} = R_2$. The different slopes arise from the different values of ℓ_{NS} in each theory. Eq. (118) does not include any spin effects, which are required in dCS and likely required in EDGB for NSs. To attempt to include these spin effects, we suppressed $\langle\dot{\omega}\rangle$ by $\chi_1\chi_2$ for dCS, and took a fiducial spin period of 300ms [30] which gives $\chi \approx 7 \times 10^{-4}$. Similarly, since the scalar quadrupole for a NS in EDGB is sourced at second order in spin, we suppressed the pericenter precession in EDGB by $\chi_1^2\chi_2^2$ when generating Fig. 2.

For comparison, ref. [19] estimated a bound $\ell_{\text{dCS}} \lesssim 10^8\text{km}$ from Solar system experiments. The pulsar bounds here are estimated to be better by 4 or more orders of magnitude. The bound we have estimated here for dCS is consistent with the calculation in ref. [12]. However, this estimated bound must be interpreted with caution. Notice in Fig. 1 that when $\ell \sim 30\text{km}$ or larger, an isolated neutron star will be in the large-modification regime. However, the bounds estimated here were calculated with the mass, radius, and multipole structure of the constituent neutron star. While it should be safe to use the scaling of these properties in the small-modification regime, it is not clear that these parameters scale as assumed into the large-modification regime. This means these estimated bounds may not be robust.

B. Gravitational wave bounds

We now return to a binary inspiral detected through gravitational waves with some given signal/noise ratio

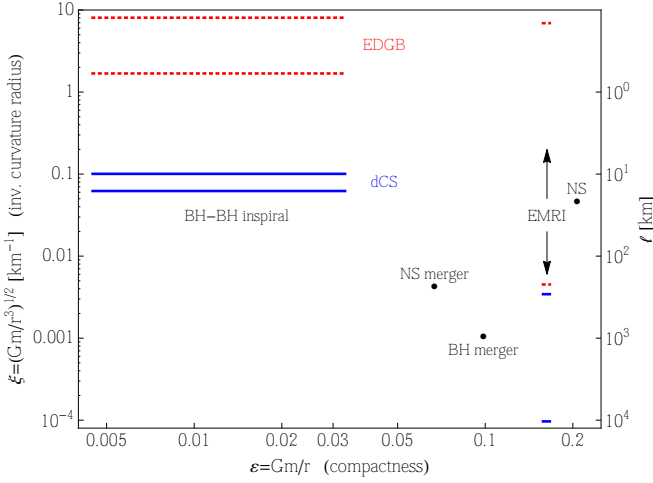


FIG. 3. (Color online) Estimated bounds on ℓ from gravitational wave measurements. This Figure is the dashed region within Fig. 2. Solid (blue online) lines correspond to dCS, dotted (red online) lines correspond to EDGB. Estimated bounds from a BH-BH inspiral in LIGO appear at left, with the horizontal extent of the line representing the range of frequencies in band. Estimates from an EMRI detected in LISA with the small body being a black hole appear at right—they evolve through a narrower frequency range.

(SNR). After a detection, to properly bound ℓ in some given theory [with values given for $(|\epsilon|, d, r, \ell_{\text{NS}}, \ell_{\text{BH}})$] would involve integrating against templates that include all the corrections in Sec. VIII and treating ℓ as a free parameter. However, from the work of [31] we can make a simple estimate of the bounds which could be placed. Their Eq. (20) estimates a bound

$$|\beta| \lesssim \frac{3}{\text{SNR} \Delta u^b} \quad (119)$$

where we have defined the shorthand $\Delta u^b \equiv |u_{\text{min}}^{b_{\text{ppE}}} - u_{\text{max}}^{b_{\text{ppE}}}|$, with $u = \pi G M f = \eta^{3/5} v^3$, the min and max referring to the frequency range where the signal is in band. This can be directly converted into bounds on ℓ from either the $\beta^{(1)}$ effect given in Eq. (117c) or the $\beta^{(3)}$ effect given in Eqs. (117d)-(117g). For example, for the $\beta_{\text{ppE}}^{(1)}$ bound we find [compare with Eq. (118)]

$$\ell^{2+2\varphi} \lesssim \frac{3}{\text{SNR} \Delta u^{b^{(1)}}} \frac{\eta^{+1+4s/5}}{C_1^r C_2^r} (Gm)^2 R_1^\varphi R_2^\varphi \left[\frac{(Gm)^2}{R_1 R_2} \right]^s. \quad (120)$$

Meanwhile, for $\beta_{\text{ppE}}^{(3)}$ we find the simple expressions

$$\ell^{2+2\varphi} \lesssim \frac{3\eta^{(12+6\varphi)/5}}{\text{SNR} \Delta u^{b^{(3)}}} (Gm)^{2+2\varphi} \left(\frac{m}{\delta m} \right)^2 \quad (s - \varphi = -1) \quad (121a)$$

$$\ell^{2+2\varphi} \lesssim \frac{3\eta^{(8+6\varphi)/5}}{\text{SNR} \Delta u^{b^{(3)}}} (Gm)^{2+2\varphi} \left(\frac{m}{\delta m} \right)^2 \quad (s - \varphi = 0) \quad (121b)$$

$$\ell^{2+2\varphi} \lesssim \frac{3\eta^{(4+6\varphi)/5}}{\text{SNR} \Delta u^{b^{(3)}}} (Gm)^{2+2\varphi} \quad (s - \varphi = +1) \quad (121c)$$

$$\ell^{2+2\varphi} \lesssim \frac{3\eta^{(10+6\varphi)/5}}{\text{SNR} \Delta u^{b^{(3)}}} (Gm)^{2+2\varphi} \left(\frac{m}{\delta m} \right)^2. \quad (s - \varphi = +2) \quad (121d)$$

To generate the estimated bounds in Fig. 3 we considered two systems, two theories, and both $\beta^{(1)}$ and $\beta^{(3)}$, for a product of 8 estimated constraints. Each constraint came from assuming an SNR 30 detection, i.e. that β could be bounded at the level of

$$|\beta| \lesssim \frac{0.1}{\Delta u^b}.$$

The two theories under consideration are dCS, represented as a solid line (blue online), and EDGB, represented as a dotted line (red online) with the parameters given in Table I. The two systems under consideration were a stellar mass BH-BH inspiral detected in LIGO, and an EMRI detected in LISA where the small object is a BH. For the stellar mass BH-BH system we took fiducial parameters $m_1 = 10M_\odot$ and $m_2 = 11M_\odot$. We represent the frequency range during which the inspiral is in band as the horizontal extent of the line, roughly 20Hz-400Hz. The BH-BH LIGO estimates appear in the left of the figure. For the EMRI system we took parameters $m_1 = 10^6 M_\odot$, $m_2 = 10M_\odot$. The frequency range ends when the small body plunges, at a compactness of $\epsilon = 1/6$, and starts 1 year before plunge. Since an EMRI evolves very slowly, the frequency range is quite narrow. These estimates appear in the right of the figure. We took all BHs to be rapidly spinning so that there is no spin suppression in dCS.

The same expression [Eq. (120)] is used for all of the $\beta^{(1)}$ constraints, just with different parameters and different values of b_{ppE} . Further the $\beta^{(3)}$ expressions depend on the difference $s - \varphi$, which differs for the combinations of theories and systems. For dCS we have $s - \varphi = 0$, given by Eq. (121b). In EDGB, we $s - \varphi = -1$ for a BH-BH binary, given by Eq. (121a) [for a NS-NS (not considered here) we would have $s - \varphi = +1$]. For dCS we have $b_{\text{ppE}} = -1/3$ in all cases, whereas in EDGB we must use $b_{\text{ppE}}^{(1)} = -5/3$ and $b_{\text{ppE}}^{(3)} = -7/3$. For the combination of dCS and stellar mass BHs, the constraint coming from $\beta^{(1)}$ is stronger than the $\beta^{(3)}$ constraint (and so is higher up in Fig. 3). For all other combinations of theories and systems, the situation is reversed and the $\beta^{(3)}$ bound is stronger.

Now, let us compare the estimated bounds from GW observations shown in Fig. 3 with those from previous works [11, 20, 27, 32]. The estimated GW bounds on EDGB found here are slightly stronger than the previously estimated bounds from [11, 20]. This is because in this Paper, we did not take correlations among model parameters into account, whereas constraints from previous works are either based on a Bayesian [11, 31] or a Fisher analysis [20], which weakens the bounds due to parameter correlations. However, as an order of magnitude estimate, our results are consistent with refs. [11, 20].

For the bounds on dCS, the one from a BH-BH inspiral is of the same order as the one estimated in [27], where the authors performed a Fisher analysis and included other corrections that we do not take into account in this paper. On the other hand, the EMRI bound is larger than the one estimated in [32] by more than one order of magnitude. This is because the latter considered a dCS correction due to the modification in the gravito-magnetic component of the metric to linear order in the BH spin, which is of higher pN order than the one considered in this paper (2pN effect). Finally let us reiterate the caveat raised at the end of Sec. IX A, now relevant for the estimated dCS bound coming from EMRIs. This analysis used the mass and multipole structure of the small black hole, but the multipoles may not scale as expected into the strong-modification regime. Therefore the dCS EMRI bound, which is not smaller than kilometer scale, may not be robust.

X. CONCLUSION

In this Paper, we have connected observables—pulsar binary pericenter precession, and binary gravitational wave phase—to the physical structure of the theory in a large class of models which includes Einstein-dilaton-Gauss-Bonnet and dynamical Chern-Simons. We have estimated upper limits which one would find from observations consistent with general relativity, from both pericenter precession and gravitational waves. Both bounds are expected to be orders of magnitude better than Solar system bounds, with gravitational waves being between 1 and 8 orders of magnitude better than pulsar timing (depending on the compactness of the pulsar binary). The typical length scale for gravitational-wave bounds is estimated to be $\ell \lesssim 10\text{km}$.

To perform these calculations, we have parameterized the non-minimal interaction Lagrangian \mathcal{L}_{int} in terms of the new length scale ℓ , which acts as a coupling parameter, and in terms of the presence/absence of parity violation $|\epsilon|$, the number of derivatives in the interaction d , and the number of curvature invariants r . We also parameterized the scalar field sourced by compact bodies in terms of the leading non-vanishing multipole number, ℓ_{NS} and ℓ_{BH} . We have estimated the multipole moments μ^Q from scaling arguments, which agree with asymptotic matching to strong-field calculations for known examples. We

treat the compact objects with post-Newtonian theory by describing them as effective point particles with scalar hair. This allows us to derive an effective scalar multipole-multipole interaction Lagrangian $L_{\text{int}}[\mathbf{x}_1, \mathbf{x}_2]$ and compute the pericenter precession in a compact binary system. We also computed the scalar multipole moments of the binary and thus the radiative scalar field and energy loss.

We used the stationary phase approximation to compute the modification to the gravitational wave phase, by combining the modified binding energy, modified Kepler relation, and the corrected energy loss. This we connect to parameters in the parameterized post-Einsteinian (ppE) framework: the b and β parameters arising from four distinct effects. These effects are from i) the conservative scalar interaction, ii) the conservative metric deformation, iii) the energy lost in scalar radiation, and iv) the correction to the energy lost in gravitational waves.

From both the pericenter precession and gravitational wave calculations we can estimate the bound that would be placed from observations consistent with general relativity (Fig. 2). These bounds are estimated to be orders of magnitude better than Solar system constraints. The gravitational wave bounds are between 1 and 3 orders of magnitude better than those arising from highly precessing pulsar binary systems (depending on the compactness of the system). The typical length scale for gravitational-wave bounds is estimated to be $\ell \lesssim 10\text{s}$ of km.

However, these estimates must be interpreted cautiously. For some range of ℓ , a constituent compact body may be in the large-correction regime of the theory even though the binary is in the small-correction regime, so these bounds may not be robust.

In this work we have captured only the scalar effects in the theories we considered. Though we parameterized some of the metric effects, we were unable to say how they scaled and thus unable to determine what kinds of bounds they could provide. Another possible extension of this present work would be to determine how these metric effects generically scale.

Further, this work has only considered theories with a metric and a massless scalar field. Although this includes a large class of theories, there are many more types of theories which are not included. Some examples are bimetric theories [33] and tensor-vector or tensor-vector-scalar [34] theories. In particular, here we can not capture any Lorentz-violating effects present in a theory such as Einstein-Æther [35]. Additionally, the multipole structure in tensor-vector and especially Lorentz-violating theories is likely much richer than what is possible in a scalar-tensor theory. Extending this work to include these effects is a straightforward avenue for future investigation.

ACKNOWLEDGMENTS

This work was inspired by a discussion at the *Gravitational Wave Tests of Alternative Theories of Gravity in the Advanced Detector Era* workshop at MSU, and

sharpened by discussions at a long-term workshop at the Yukawa Institute for Theoretical Physics at Kyoto University. We would like to acknowledge the organizers of both workshop for creating programs that encouraged interaction and for their hospitality during the programs. We would like to thank É. Flanagan and N. Yunes for useful discussion. LCS acknowledges that support for this work was provided by the National Aeronautics and Space Administration through Einstein Postdoctoral Fellowship Award Number PF2-130101 issued by the Chandra X-ray Observatory Center, which is operated by the Smithsonian Astrophysical Observatory for and on behalf of the National Aeronautics Space Administration under contract NAS8-03060, and further acknowledges support from NSF grant PHY-1068541. KY acknowledges support from NSF grant PHY-1114374, NSF CAREER Grant PHY-1250636 and NASA grant NNX11AI49G.

Appendix A: Relation between ℓ and cutoff

In this work we have parameterized the non-minimal interaction term \mathcal{L}_{int} through the length scale ℓ . However, in the EFT framework, this term should arise from integrating out some unknown physics above an energy scale Λ , the cutoff of this effective theory. With the physics above this energy scale unknown, naturalness arguments are typically invoked to estimate the sizes of irrelevant/marginal/relevant operators in the action. Here we can recast the action given in Eq. (1) in terms of Λ . This is useful for estimating quantum corrections, though in this paper we have treated everything classically.

First, we must rewrite the Einstein-Hilbert term in terms of a canonically normalized field variable. The Ricci scalar is expanded as

$$R \sim (\partial h)^2 + \partial^2 h. \quad (\text{A1})$$

The E-H term, $\mathcal{L}_{\text{EH}} \sim m_{\text{pl}}^2 R$, becomes canonical by absorbing one power of m_{pl} into h , i.e. defining

$$h^{\text{can}} \equiv m_{\text{pl}} h, \quad (\text{A2})$$

so that $\mathcal{L}_{\text{EH}} \sim (\partial h^{\text{can}})^2$. Here h^{can} has canonical length dimensions, i.e. $[h^{\text{can}}] = [L]^{-1}$.

Performing this redefinition in the interaction Lagrangian gives

$$\mathcal{L}_{\text{int}} \sim \frac{(m_{\text{pl}} \ell) \ell^{\mathcal{P}}}{m_{\text{pl}}^{2r}} \theta T[\epsilon^{0,1}, \partial^d, (\partial h^{\text{can}})^{2r}]. \quad (\text{A3})$$

Now that all fields in this term are canonically normalized, from naturalness we will argue that the coefficient of this term should be an $\mathcal{O}(1)$ number times an inverse power of the cutoff Λ . Specifically, for dimensional correctness we must have

$$\mathcal{L}_{\text{int}} \sim \frac{c_1}{\Lambda^{4r+d-3}} \theta T[\epsilon^{0,1}, \partial^d, (\partial h^{\text{can}})^{2r}] \quad (\text{A4})$$

where c_1 is some coefficient of order unity. This alternate parameterization in terms of c_1/Λ^{4r+d-3} is just as valid as the one in terms of $(m_{\text{pl}} \ell) \ell^{\mathcal{P}}$. Immediately we have the relation between Λ and ℓ ,

$$\Lambda \sim c_2 \left[m_{\text{pl}}^{(2r-1)} \ell^{-(2r+d-2)} \right]^{1/(4r+d-3)} \quad (\text{A5})$$

with c_2 another order-unity coefficient. We see that the cutoff is parametrically between the inverse-length $1/\ell$ and the Planck scale m_{pl} .

For example, in both EDGB and dCS we have the scaling

$$\Lambda \sim c_2 m_{\text{pl}}^{3/5} \ell^{-2/5}. \quad (\text{A6})$$

In terms of energies,

$$1\text{km}^{-1} \approx 2 \times 10^{-10} \text{eV}.$$

This gives an order of magnitude for the cutoff energy

$$\Lambda \sim c_2 \cdot 3\text{TeV} \left(\frac{\ell}{10\text{km}} \right)^{-2/5}.$$

From Fig. 1 we see that for the endpoint of a NS-NS merger to be within the regime of validity we should have $\ell \lesssim 400\text{km}$ in dCS and EDGB. This translates, with the above, into having a cutoff at least as large as $\Lambda \gtrsim 0.7\text{TeV}$. If we want the structure of a NS to be within the small-correction regime, then we see again from Fig. 1 that we want $\ell \lesssim 30\text{km}$. This corresponds to a cutoff at least as large as $\Lambda \gtrsim 2\text{TeV}$.

[1] C. M. Will, *Theory and Experiment in Gravitational Physics*, 2nd ed. (Cambridge University Press, Cambridge; New York, 1993).
[2] C. M. Will, *Living Reviews in Relativity* **9** (2006), 10.12942/lrr-2006-3.
[3] F. Moura and R. Schiappa, *Class.Quant.Grav.* **24**, 361 (2007), arXiv:hep-th/0605001 [hep-th].
[4] P. Pani and V. Cardoso, *Phys.Rev.* **D79**, 084031 (2009), arXiv:0902.1569 [gr-qc].
[5] R. Jackiw and S. Pi, *Phys.Rev.* **D68**, 104012 (2003),

arXiv:gr-qc/0308071 [gr-qc].
[6] S. Alexander and N. Yunes, *Phys.Rept.* **480**, 1 (2009), arXiv:0907.2562 [hep-th].
[7] T. Damour, in *Gravitational Radiation*, edited by N. Deruelle and T. Piran (1983) p. 58.
[8] L. Blanchet, *Living Reviews in Relativity* **9** (2006), 10.12942/lrr-2006-4.
[9] C. R. Galley and B. Hu, *Phys.Rev.* **D79**, 064002 (2009), arXiv:0801.0900 [gr-qc].
[10] J. K. Bloomfield and E. E. Flanagan, *JCAP* **1210**, 039

- (2012), arXiv:1112.0303 [gr-qc].
- [11] K. Yagi, L. C. Stein, N. Yunes, and T. Tanaka, Phys. Rev. D **85**, 64022 (2012), arXiv:1110.5950 [gr-qc].
- [12] K. Yagi, L. C. Stein, N. Yunes, and T. Tanaka, Phys. Rev. D **87**, 84058 (2013), arXiv:1302.1918 [gr-qc].
- [13] S. E. Gralla, Phys. Rev. D **87**, 104020 (2013), arXiv:1303.0269 [gr-qc].
- [14] K. S. Thorne, Reviews of Modern Physics **52**, 299 (1980).
- [15] L. Blanchet and T. Damour, Royal Society of London Philosophical Transactions Series A **320**, 379 (1986).
- [16] C. M. Will and A. Wiseman, Phys. Rev. D **54**, 4813 (1996), arXiv:gr-qc/9608012 [gr-qc].
- [17] N. Yunes and L. C. Stein, Phys. Rev. D **83**, 104002 (2011), arXiv:1101.2921 [gr-qc].
- [18] N. Yunes and F. Pretorius, Phys. Rev. D **79**, 84043 (2009), arXiv:0902.4669 [gr-qc].
- [19] Y. Ali-Haïmoud and Y. Chen, Phys. Rev. D **84**, 124033 (2011), arXiv:1110.5329 [astro-ph.HE].
- [20] K. Yagi, Phys. Rev. D **86**, 081504 (2012), arXiv:1204.4524 [gr-qc].
- [21] L. Blanchet and B. R. Iyer, Phys. Rev. D **71**, 024004 (2005), arXiv:gr-qc/0409094 [gr-qc].
- [22] W. M. Smart, *Celestial mechanics*. (London, New York, Longmans, Green [1953], 1953).
- [23] H. P. Robertson and T. W. Noonan, *Relativity and cosmology* (Philadelphia: Saunders, 1968).
- [24] L. C. Stein and N. Yunes, Phys. Rev. D **83**, 064038 (2011), arXiv:1012.3144 [gr-qc].
- [25] W. Tichy, E. E. Flanagan, and E. Poisson, Phys. Rev. D **61**, 104015 (2000), arXiv:gr-qc/9912075 [gr-qc].
- [26] K. Yagi, N. Yunes, and T. Tanaka, Phys. Rev. D **86**, 044037 (2012), arXiv:1206.6130 [gr-qc].
- [27] K. Yagi, N. Yunes, and T. Tanaka, Phys. Rev. Lett. **109**, 251105 (2012), arXiv:1208.5102 [gr-qc].
- [28] N. Yunes and F. Pretorius, Phys. Rev. D **80**, 122003 (2009), arXiv:0909.3328 [gr-qc].
- [29] D. R. Lorimer, Living Reviews in Relativity **11** (2008), 10.12942/lrr-2008-8.
- [30] C.-A. Faucher-Giguere and V. M. Kaspi, Astrophys. J. **643**, 332 (2006), arXiv:astro-ph/0512585 [astro-ph].
- [31] N. Cornish, L. Sampson, N. Yunes, and F. Pretorius, Phys. Rev. D **84**, 062003 (2011), arXiv:1105.2088 [gr-qc].
- [32] P. Canizares, J. R. Gair, and C. F. Sopuerta, Phys. Rev. D **86**, 044010 (2012), arXiv:1205.1253 [gr-qc].
- [33] S. Hassan and R. A. Rosen, JHEP **1202**, 126 (2012), arXiv:1109.3515 [hep-th].
- [34] J. D. Bekenstein, Phys. Rev. D **70**, 083509 (2004), arXiv:astro-ph/0403694 [astro-ph].
- [35] T. Jacobson, PoS **QG-PH**, 020 (2007), arXiv:0801.1547 [gr-qc].